ADVANCED FUNCTIONAL MATERIALS
www.afm-journal.de

Novel Electronics for Flexible and Neuromorphic Computing

*Han Eol Lee, Jung Hwan Park, Tae Jin Kim, Doyoung Im, Jung Ho Shin, Do Hyun Kim, Baker Mohammad, Il-Suk Kang, and Keon Jae Lee**

Emerging classes of flexible electronic systems that can be attached to a wide range of surfaces from wearable clothes to internal organs have driven significant advances in communication protocols (e.g., Internet of Things, augmented reality) and clinical research, shifting today's personal computing paradigm. The field of "system on plastic" is on the verge of an innovative breakthrough toward a hypercognitive society by being fused with current neuromorphic applications in the spotlight, which can offer intelligent services such as personalized feedback therapy and autonomous driving. The novel concept of electronics for flexible and neuromorphic computing requires an important research leap in micro-/nanoelectronics on plastics, system-level integration techniques (interconnection and packaging), and synaptic devices. Here, representative advances and developments in the area of flexible and neuromorphic technologies are reviewed with regard to device configurations, materials, fabrication processes, and their potential research fields.

1. Introduction

Flexible electronics have attracted significant attention due to their outstanding portability, conformal contact characteristic, and human friendly interfaces compared to bulk silicon devices, showing considerable potential to change the paradigm of individual computing to a hyperconnected society toward the fourth industrial revolution.[1–3] For example, flexible displays can be applied to smart electronics such as Internet of Things (IoT),[4–7] augmented reality (AR),[8,9] and wearable applications[10–20] to exchange customized and bilateral information via visual communication protocols. The field of flexible electronics is being converged with artificial intelligence (AI) by providing users' biological and behavioral signals collected in wearable biodevices,[21–31] offering intelligent services based on big data cloud computing and machine learning.[32–40]

A number of research groups have demonstrated flexible memories, thin film transistors (TFTs), and integrated circuits (ICs) as key technology for data processing, information storage, and communication.[41–49] Since Kim et al.[50] reported functional flexible resistive random access memory (RRAM), various chalcogenide-based phase change memories (PCMs)[51–54] as well as RRAMs using inorganic (e.g., WO_3, Al_2O_3, HfO_2, TiO_2),[45,49,50,55–57] carbon (graphene, carbon nanotubes (CNTs)),[58–64] and organic materials[65–68] have been fabricated on polymer films. In addition, an ultrathin TFT and Si-based large-scale integration (LSI) were demonstrated for high-density flexible electronics.[8,69,70] Beyond the front-end device level, flexible packaging has been developed to interconnect core and peripheral modules to realize fully operational system-on-plastic (SoP).[71–75]

Neuromorphic computing systems (brain-inspired model of parallel neuron network) are considered as a promising technology for AI applications, overcoming the limitation of von Neumann architecture (serial and iterative processing) for intelligent data analysis and low power consumption.[76–81] With the rapid advancement in the electronics (e.g., memristor, PCM, and TFT) on plastics or any type of surface,[82–90] emulation of biological synapses (adaptive synaptic weight,[91–94] and spike-timing-dependent plasticity (STDP)[95–99] of neurons) is being demonstrated on flexible substrate, which realizes an era of merged electronics toward cognitive IoT, physiological sensor, wearable computer, and autonomous driving system.[92,100]

Here, we present recent progress in the field of electronics for flexible and neuromorphic applications that can be classified into four main categories: i) various devices (e.g., resistive memory, PCM, TFT, and IC) on plastic for computing, ii) flexible electronic systems using large-scale interconnection and packaging, iii) electronics for neuromorphic engineering, and iv) promising research areas of flexible synaptic applications. In addition, we have organized the main features of the studies in each section as a table to clearly compare their performance and challenges. The new electronic concept of a flexible and

H. E. Lee, Dr. J. H. Park, T. J. Kim, D. Im, J. H. Shin, D. H. Kim, Prof. K. J. Lee
Department of Materials Science and Engineering
Korea Advanced Institute of Science and Technology (KAIST)
291 Daehak-ro, Yuseong-gu, Daejeon 34141, Republic of Korea
E-mail: keonlee@kaist.ac.kr
Prof. B. Mohammad
Department of Electrical and Computer Engineering
Khalifa University of Science Technology and Research
Abu Dhabi 127788, United Arab Emirates (UAE)
Dr. I.-S. Kang
National Nanofab Center
Korea Advanced Institute of Science and Technology (KAIST)
291, Daehak-ro, Yuseong-gu, Daejeon 34141, Republic of Korea

DOI: 10.1002/adfm.201801690

neuromorphic system will provide a prospective outlook for soft brain–machine interface, cognitive healthcare, and intelligent wearable device.

2. Flexible Memory for Computing

2.1. Flexible Inorganic Resistive Memory

Flexible resistive memory has emerged as next-generation memory, reconfigurable logic circuit devices, and synaptic applications because of its fast response, simple structure, high scalability, low cost, and memristive switching characteristics.[57,101–105] Inorganic materials have significant merits for flexible resistive memory applications due to their excellent performance and advantages for high-density electronics. However, there are major challenges that must be confronted to overcome the inherent thermal limitation of plastic substrate (e.g., low melting point and heat shrinkage/expansion), requiring new solutions for inorganic resistive memory on plastic with outstanding properties. Kim et al.[50] reported fully functional flexible RRAM by demonstrating a one transistor–one memristor (1T–1M) SoP in a NOR type array via transfer printing process. The flexible 1T–1M array could be conformally attached on a quartz rod with a bending radius of 5 mm without causing delamination or cracking of the RRAM, as shown in **Figure 1**a. The developed flexible device presented reproducible and reliable resistive switching properties with outstanding stability upon harsh bending (Figure 1b). This crossbar-structured 1T–1M RRAM on a plastic film exhibited excellent RAM operation without cell-to-cell interference by selectively switching off the unaddressed memory cells (Figure 1c). Ji et al.[57] fabricated RRAM with a Cu/nanoporous (NP) WO_{3-x}/indium tin oxide (ITO) structure on a polyethylene terephthalate (PET) film by employing electrochemical anodic process in a room temperature (Figure 1d). As presented in Figure 1e,f, the RRAM device on a polymer substrate showed an I_{on}/I_{off} ratio of $\approx 10^5$ without serious switching failure even after 1000 cycles of 1.58% bending strain.

Recently, an inorganic-based laser liftoff (ILLO) has been developed to transfer entire inorganic devices onto plastic films to realize flexible, high-performance, and multifunctional electronics with excellent complementary metal–oxide–semiconductor (CMOS) compatibility.[24,106–113] **Scheme 1** shows the representative mechanisms of the ILLO process.[8,24,114] When a laser (e.g., excimer (XeCl)) is irradiated to the backside of the rigid substrate with a high bandgap (larger than input photon energy), light can pass through the transparent substrate, reaching to the laser absorbing material. Depending on light interacting films (e.g., lead zirconate titanate, gallium nitride (GaN), and hydrogenated amorphous Si), various photothermal interactions such as melting/vaporizing, dissociating (e.g., $2GaN_{(solid)} \rightarrow 2Ga_{(liquid)} + N_{2\ (gas)}$), and explosive gas releasing occurred in the sacrificial layer, which weaken the interfacial adhesion between the substrate and active device. This low adhesion enables ultrathin electronics to be safely peeled off from the mother substrate without any mechanical deformations, cracks, or wrinkles.

Keon Jae Lee received his Ph.D. in materials science and engineering (MSE) at the University of Illinois, Urbana–Champaign (UIUC). During his Ph.D. at UIUC, he was involved in the first coinvention of "flexible single-crystalline inorganic electronics," using top-down semiconductors and soft lithographic transfer. Since 2009, he has been a professor in MSE at the KAIST. His current research topics are self-powered flexible electronic systems including energy-harvesting/storage devices, LEDs, LSI, high-density memory, and laser–material interactions for in vivo biomedical and flexible applications.

Kim et al.[104] demonstrated one selector–one resistor (1S–1R) crossbar array (32 × 32) on a plastic film via ILLO (Figure 1g). The flexible 1S–1R memory maintained a constant resistance ratio between the low resistance state (LRS) and high resistance state (HRS) without severe degradation despite 1000 iterations of bending fatigue (15 mm bending diameter). As shown in Figure 1h, the 1S–1R memory could work effectively on a plastic film without electrical interference even in a one bit-line pull-up (OBPU) condition by suppressing unintended current paths. Precise addressing capability of flexible 1S–1R memory was additionally confirmed through successful demonstration of a 3 × 3 image based on the HRS (logic state "0") and LRS (logic state "1") currents. **Table 1** shows the main features of the aforementioned flexible inorganic resistive memories.

2.2. Carbon- and Organic-Based Resistive Memory on Plastics

Flexible resistive memory has been fabricated using various carbon and organic materials to exploit their unique electrical properties (e.g., memristive switching behaviors) and flexibility.[62,115–120] Hwang et al.[62] demonstrated mechanically flexible resistive memory by solution casting of CNT–nanocomposites (polystyrene (PS) and chemically doped CNTs), as schematically illustrated in **Figure 2**a. Figure 2b presents the current–voltage (*I–V*) characteristics of a memory device fabricated with a boron (B)-doped CNT (BCNT)–based nanocomposite. B-doping increased the deep charge traps in the PS/CNT nanocomposite, enabling an on–off ratio exceeding 10^2. As shown in Figure 2c, the flexible devices presented reliable resistive memory characteristics even after being bent more than 500 times. In 2013, flexible nonvolatile memory (NVM) based on graphene oxide (GO) material (highly reduced GO (hrGO)/lightly reduced GO (lrGO)/hrGO) was demonstrated (Figure 2d). Voltage was applied to the top and bottom hrGO

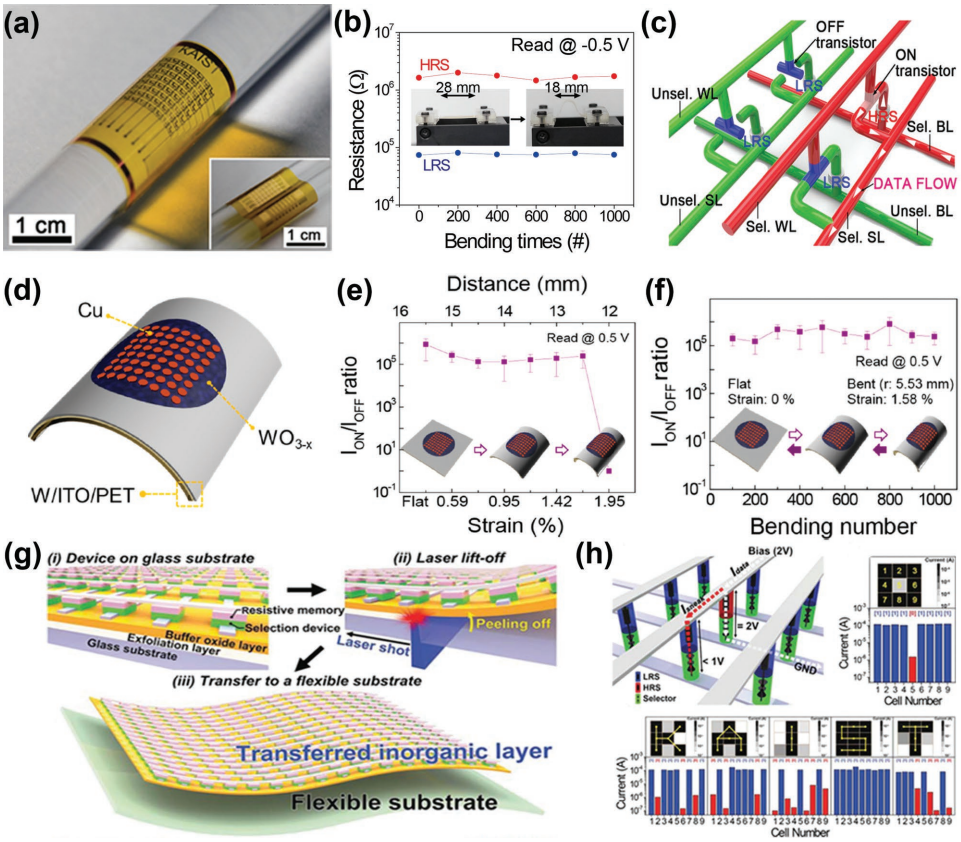

Figure 1. a) Photograph of 1T–1M-system-based flexible RRAM array attached on a quartz rod. The inset shows that the flexible RRAM can provide conformal contact on the curved surfaces of two pipets. b) Mechanical durability test of the flexible RRAM. The insets present the straightening and bending of the devices. c) Schematic of the structure of the flexible 1T–1M RRAM. The green and red lines represent unselected and selected, respectively. The white arrows indicate a data flow related to the state of the (2,2) cell. d) Schematic of the flexible Cu/nanoporous (NP) WO_{3-x}/ITO RRAM. e) I_{on}/I_{off} ratio distribution of the flexible Cu/nanoporous (NP) WO_{3-x}/ITO RRAM under different bending conditions. f) Bending fatigue test of the flexible Cu/nanoporous (NP) WO_{3-x}/ITO RRAM during 1000 bending/unbending cycles. g) Schematic of the flexible 1S–1R RRAM fabrication via the inorganic-based laser liftoff (ILLO). h) Operation of the flexible 1S–1R RRAM in the one bit-line pull-up (OBPU) condition: schematic of the device operation in the OBPU condition (top left), and the addressing test results of the flexible 1S–1R RRAM based on the histograms of currents with 3×3 images, and the corresponding color maps (top left, bottom). (a–c) Reproduced with permission.[50] Copyright 2011, American Chemical Society. (d–f) Reproduced with permission.[57] Copyright 2016, American Chemical Society. (g, h) Reproduced with permission.[104] Copyright 2014, Wiley-VCH.

electrodes to control the resistance state of the flexible device, presenting a NVM effect. The hrGO/lrGO/hrGO NVM structure on PET showed a strong retention ability (≈10^3 s) without significant device degradation. Flexible graphene/SiO_x/graphene NVM with a crossbar structure was also demonstrated by utilizing a graphene transfer process, as presented in Figure 2e. A fluoropolymer film with a high-melting point (>280 °C) was used as a substrate to withstand the current local heating effect that could be induced during the initial electroforming step of the resistive memory on plastic. The electroformed memory exhibited a reliable on and off switching characteristic (ratio over 10^4) without degradation of the memory state during 300 cycles of bending, which shows the feasibility of flexible memory applications (Figure 2f). Nagashima et al.[121] reported nonvolatile RRAM on plastic based on Ag-decorated cellulose nanofiber paper (Ag-CNP). The flexible Ag-CNP memory could conformally wrap the glass rod without any crack and exfoliation of the device, as shown in Figure 2g. The developed flexible memory presents the stable on–off resistance ratio of 10^6 at severe bending strain (radius of 350 μm) due to outstanding mechanical properties (e.g., high tensile strength, low thermal expansion coefficient) of CNP (Figure 2h). Kim and Lee[122] proposed a flexible biopolymer-based RRAM on plastic using carboxymethyl κ-carrageenan (CM:κ-car) solution casting. The CM:κ-car material with high oxygen vacancy and conductivity enabled a low power resistive switching (≈0.35 μW). In addition, the flexible device exhibited a fast switching speed (50 ns), low reset voltage (≈0.05 V), and stable operation under compressive/tensile stress, as shown in Figure 2i (Refer to **Table 2**).

2.3. Flexible Phase-Change Memory

PCM has recently won attention due to the commercialization of Intel's 3D XPoint PCM.[123,124] PCM on flexible film has strong potential for future memory devices because of its excellent endurance, high switching speed, remarkable scalability, and analog conductance change characteristic.[125,126] However, it was difficult to fabricate high-density PCM on a

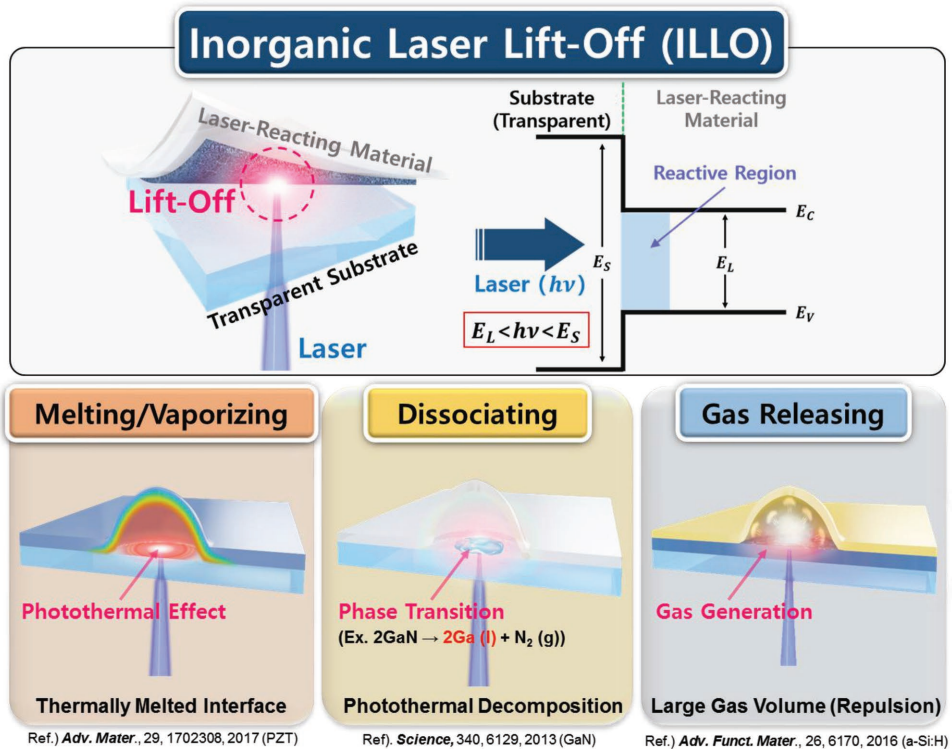

Scheme 1. The principle and exfoliation mechanisms of the ILLO.

flexible substrate with excellent performance because of its nonflat feature and vulnerability to chemical elements.[127,128] Although various soft lithography and printing techniques have been established as chemical-free and low temperature processes, they still have limitations in achieving high critical dimension resolution. Hong et al.[51] reported PCM with high-density nanopillars (diameter of 200 nm) on various flexible films, including PET, polyimide (PI), and stainless-steel plate via nanoimprinting lithography, as schematically presented in **Figure 3**a. The PCM with germanium–antimony–tellurium (GST) nanopillars showed an ≈10^2 current on/off ratio regardless of the type of flexible film, as confirmed by conductive atomic force microscopy. A similar nanoimprinting strategy was employed using an anodic alumina oxide (AAO) template for high-density flexible PCM. Figure 3b shows that PCM with closely packed GST nanopillars (diameter of ≈300 nm and thickness of 100 nm) could be formed on PI without severe polymer damage, exhibiting a current on/off ratio of 10^2, as presented in Figure 3c.

A large writing current has been a major obstacle for demonstrating high-performance flexible PCM because it generates intense Joule heating that causes thermal degradation of the

Table 1. Summary of main parameters in inorganic-based flexible resistive switching memories.

Fabrication process	Memory structure	Switching element	I_{on}/I_{off} ratio (@read voltage)	Operation voltage	Endurance [switching #]	Retention [s]	Bending radius [mm]	Bending cycles [#]	Opportunities	Challenges	Reference
Direct fabrication on PI + dry transfer of Si	Al/TiO_2/Al	Si-based transistor	50 (@−0.5 V)	(Set) −4.5 V (Reset) 5.5 V	100	104	8.4	1000	– Low sneak current – Random accessibility	– Low integration density – Inefficient transfer process	[50]
Semiconductor process + laser liftoff (LLO)	Pt/NiO_x/Ni	Nonlinear resistor (Ni/TiO_2/Ni)	>500 (@2 V)	(Set) −4.2 V (Reset) 3 V	100	104	>5	1000	– Low sneak current – Random accessibility – High scalability		[104]
Direct fabrication on PET	Cu/WO_{3-x}/ITO	–	10^5 (@0.5 V)	(Set) 1 V (Reset) −1.1 V	1000	5×10^5	5.53	1000	– Facile fabrication	– Lack of interconnection	[57]

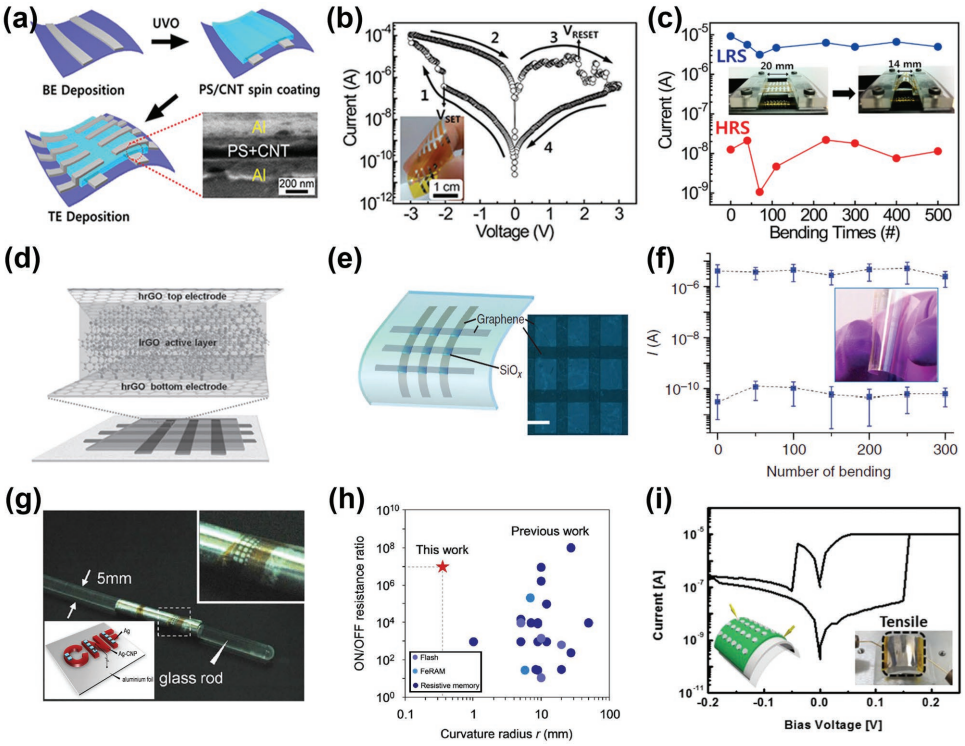

Figure 2. a) Schematic and scanning electron microscope (SEM) image of the CNT nanocomposite–based flexible resistive memory. b) *I*–*V* characteristic of the memory device fabricated with nanocomposite composed of boron (B)-doped CNTs. The inset shows the device under the bending condition. c) Current measurement of the CNT–nanocomposite-based flexible memory during 500 bending/unbending cycles. The insets show the memory device under two different bending conditions. d) Schematic of the flexible nonvolatile resistive memory (NVM) device based on graphene oxide (GO) with a configuration of highly reduced GO (hrGO)/lightly reduced Go (lrGO)/hrGO. e) Schematic of the flexible graphene/SiO_x/graphene crossbar-structured NVM on a plastic substrate. The inset shows an optical image of the device structure. f) Bending fatigue test of both ON/OFF memory devices during 300 bending/straightening cycles at bending diameter curvature of ≈1.2 cm. The inset shows the memory device under the bending condition. g) Photograph of the flexible Ag–CNP-based RRAM providing conformal contact on the curved surface of a glass rod. The insets present the magnified view of the device (top right), and the schematic of the fabricated flexible RRAM devices (bottom left). h) On–off resistance ratio of the flexible Ag–CNP memory depending on the bending curvature. i) Resistive-switching property of CM:κ-car-based flexible RRAM under tensile bending condition. (a–c) Reproduced with permission.[62] Copyright 2012, American Chemical Society. (d) Reproduced with permission.[116] Copyright 2013, Wiley-VCH. (e, f) Reproduced with permission.[60] Copyright 2012, Springer Nature. (g, h) Reproduced with permission.[121] Copyright 2014, Springer Nature. (i) Reproduced with permission.[122] Copyright 2018, American Chemical Society.

plastic substrate and adjacent cells during PCM operation.[129] The writing current of PCM can be reduced by diminishing the switching volume of the PCM. However, it is difficult to apply conventional photolithography on rough flexible films because of the limitation in high-precision focusing and multi-level alignment.[52] Mun et al.[52] demonstrated a flexible one diode–one PCM (1D–1P) array with low operating current by incorporating block copolymer (BCP) self-assembly (Figure 3d). Si-containing poly(styrene-*b*-dimethylsiloxane) (PS-*b*-PDMS) BCPs were introduced onto GST and converted to thermally stable silicon oxide (SiO_x, thickness of 20 nm) to decrease the contact area between the phase-changing material and the heater (titanium nitride). Figure 3e and its inset clearly show fingerprint-like 20 nm width insulating SiO_x nanopatterns with 50% area fill factor, which effectively reduces the writing current of PCMs on plastic by 4 times compared to PCM without BCP. As shown in Figure 3f, a flexible BCP-incorporated PCM (f-BPCM) with a single-crystal silicon diode could be successfully switched from LRS (crystalline) to HRS (amorphous) with a rectifying characteristic of the selection device. Main parameter properties of the flexible PCM devices are indicated in **Table 3**.

3. Flexible TFTs and ICs

Flexible TFTs (e.g., Si- and oxide-based, or organic transistors) have provided considerable impacts for the commercialization of wearable electronics, currently expanding their fields to the synaptic applications by pursuing computation in a single device with high scalability and low power consumption.[19,44,130] Low-temperature polycrystalline-silicon (LTPS) TFTs are one of the most promising technologies that can be employed for next-generation electronics due to their high carrier mobility, stability, and CMOS compatibility.[131] **Figure 4**a shows the photographic and schematic (inset) images of TFTs on plastic demonstrated by LTPS.[132] Appropriate energy density (560 mJ cm^{-2}) of excimer laser was applied to completely melt the silicon while minimizing the protrusion of poly-Si created during LTPS process, resulting in flexible TFTs with

Table 2. Summary of main parameters in organic-based flexible resistive switching memories.

Fabrication process	Memory structure	I_{on}/I_{off} ratio (@read voltage)	Operation voltage	Endurance [switching #]	Retention [s]	Bending radius [mm]	Bending cycles [#]	Opportunities	Challenges	Reference
Direct fabrication on PET + graphene transfer	Graphene/SiO_2/graphene	$<10^3$ (@1 V)	(Set) 6 V (Reset) 14 V	400	–	12	300	– High transparency	– No selection device – High operation voltage	[60]
Direct fabrication on PET	Al/PS–BCNT/PS–N-doped CNT (NCNT)/Al	4×10^2 (@–1 V)	(Set) –3 V (Reset) 3 V	500	105	–	500	– Multilevel resistance – Cost-efficient process	– No selection device	[62]
Direct fabrication on PET + graphene oxide transfer by PMMA[a)]	hrGO[b)]/lrGO[c)]/hrGO	1.57×10^2 (@1 V)	(Set) –13.2 V (Reset) –	–	103	–	1000	– Eco-friendly material	– No selection device – Write-once operation – Low productivity	[116]
Direct fabrication on Al foil	Ag/Ag-decorated CNP[d)]/Pt	10^6 (@0.01 V)	(Set) 0.28 V (Reset) –0.22 V	100	105	≥0.35	103	– High flexibility	– Lack of interconnection – Unstable HRS cell resistance	[121]
Direct fabrication on PET	Ag/Ag-doped CM:κ-car[e)]/Pt	$>10^3$ (@0.02 V)	(Set) 0.2 V (Reset) –0.07 V	–	103	15	–	– Low-power operation	– Lack of interconnection – Insufficient bending robustness	[122]

[a)]PMMA: poly(methyl methacrylate); [b)]hrGO: highly reduced graphene oxide; [c)]lrGO: lightly reduced graphene oxide; [d)]CNP: cellulose nanofiber paper; [e)]CM:κ-car: carboxymethyl kappa carrageenan.

high mobility (over 45 $cm^2\ V^{-1}\ s^{-1}$) and flexibility. Lee et al.[8] demonstrated high-performance, ultrathin (4 μm thickness) oxide TFT array (50 × 50) with outstanding transparency (83%) via the ILLO process, as schematically illustrated in Figure 4b. Through the optimized ILLO based on a XeCl laser, skin-like indium zinc oxide TFTs with outstanding effective mobility of ≈40 $cm^2\ V^{-1}\ s^{-1}$ and stability under optical stress were fabricated without structural and thermal damage (Figure 4c). The flexible TFT array could be stably attached onto fabrics (Figure 4d) and reliably operated during 5000 cycles of repeated bending/unbending fatigue at a bending radius of 7.5 mm without severe mechanical (e.g., wrinkling, delamination, cracking) or electrical degradation. Furthermore, n-channel metal–oxide–semiconductor field-effect transistor (NMOS) logic inverter circuits were devised on transparent and ultrathin PET substrate, exhibiting excellent static and dynamic electrical performance. Figure 4e presents the schematic illustration of the ultrathin (total thickness of 2 μm) and imperceptible organic field-effect transistor (OFET).[133] The active device was placed between the polymer foil and encapsulation layer (near the neutral plane position) to maximize the mechanical stability. The transfer curve of the flexible OFET exhibits saturation mobility of 3 $cm^2\ V^{-1}\ s^{-1}$, presenting equal performance to that of device demonstrated on Si/SiO_2 substrate (Figure 4f). Due to the ultrathin feature of the organic transistor, it could withstand severe bending fatigue (radii of 5 μm) and crumpling stress without degradation of electrical properties (Refer to **Table 4**).

LSI (more than thousands of integrated nanocircuits) for high-density memories and core logic processors is essential to realize fully functional electronics for data analysis, storage, and communication.[134,135] Flexible LSI (f-LSI) has attracted considerable interest for intelligent computing devices on plastics.[136–138] However, there are significant difficulties of multilayer interconnection and nanoscale alignment caused by thermal expansion of polymer substrates.[69,139] Hwang et al.[69] first reported ultrathin, Si (single crystalline)-based radio frequency integrated circuits (RFICs) fabricated by a 0.18 μm CMOS process for LSI computing circuits. Figure 4g presents completely bent flexible RFIC encapsulated by liquid crystal polymer (LCP) substrates that is a promising biocompatible material for in vivo applications. The microscopic image of the IC device is shown in Figure 4h. The switching nanotransistors on plastic exhibited an effective on/off ratio of 10^8, mobility (μ_{eff}) of 400 $cm^2\ V^{-1}\ s^{-1}$, and threshold voltage of 0.26 V. In 2016, a Si-based NAND flash memory on plastic was further demonstrated by bonding Si NAND on a glass substrate and sequentially removing the handle wafer via chemical mechanical polishing and etching process (Figure 4i).[72] The aforementioned f-LSIs were successfully realized without problematic nanofabrication or multialignment steps since the LSI was initially devised on a bulk wafer and the ultrathin LSI layer was specifically transferred onto a flexible substrate.

4. Flexible Interconnection and Packaging

Packaging technology is a semiconductor back-end process that enables the assembly of core and peripheral electronics

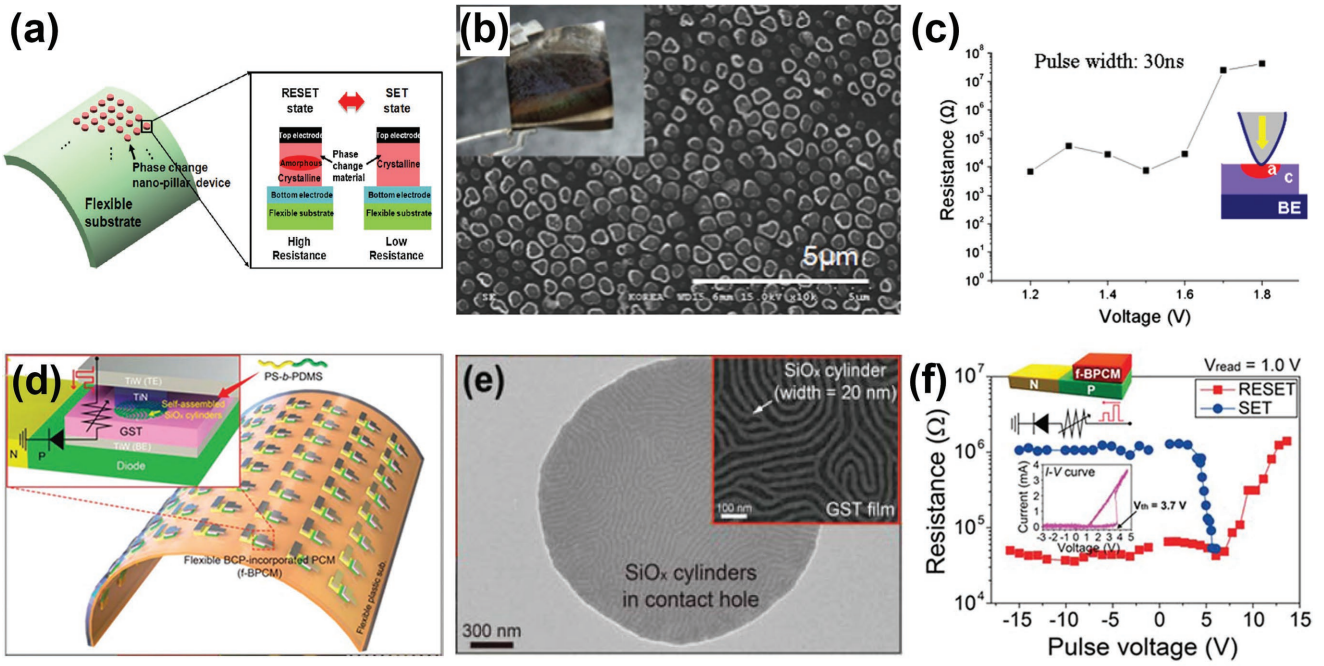

Figure 3. a) Schematic of the PCM with high-density nanopillars on flexible substrates. The inset shows the resistance change of the nanopillar phase-change material in the flexible PCM. b) SEM image of the closely packed GST nanopillar formed on the PI substrate using an AAO template in the flexible PCM. c) *R–V* characteristics of the flexible PCM fabricated by using the AAO template. d) Schematic of the flexible 1D–1P PCM array based on block copolymer (BCP) self-assembly. The inset shows the device structure of the flexible BCP-incorporated PCM (f-BPCM). e) SEM image of SiO_x nanopatterns within 2 μm diameter contact hole of f-BPCM. The inset shows a magnified SEM image of the SiO_x nanopatterns (20 nm width). f) *R–V* curves of the f-BPCM with a single-crystal Si diode at the forward and reverse pulse voltages and the corresponding circuit diagram. The inset shows the *I–V* curves of the flexible 1D–1P device. (a) Reproduced with permission.[51] Copyright 2011, Elsevier. (b, c) Reproduced with permission.[53] Copyright 2010, Elsevier. (d–f) Reproduced with permission.[52] Copyright 2015, American Chemical Society.

(e.g., memory, LSI, and sensor) for electrical interconnection and mechanical protection from the external environment.[140–142] Flexible packaging is a critical issue to be addressed for the industrial commercialization of fully operational electronic SoPs.[143,144] Kim et al.[72] reported that roll-based flexible packaging technology with fine optical alignment enabled Si-based f-NAND flash memory to be simultaneously interconnected and transferred to a flexible printed circuit board via anisotropic conductive film (ACF) bonding (**Figure 5**a). The flexible ACF packaging provides excellent electrical and resilient properties under bending stress by interconnecting vertically aligned conductors through conductive particles that are uniformly

Table 3. Summary of main parameters in flexible phase change memories.

Fabrication process	Memory structure	Switching element	I_{on}/I_{off} ratio (@read voltage)	Operation voltage	Endurance [switching #]	Retention [s]	Bending radius [mm]	Bending cycles [#]	Opportunities	Challenges	Reference
Direct fabrication on plastics + nanoimprint lithography (NIL)	Pt probe/ $Ge_2Sb_2Te_5$/ TiW	–	$>10^3$	(Set) 1.7 V (Reset) –	–	–	–	–	– High-resolution pattern of NIL process	– No selection device and interconnection – Insufficient memory performance – Incompatible with semiconductor process	[53]
	Cr/$Ge_2Sb_2Te_5$/ TiW	–	$>10^2$	(Set) 1.9 V (Reset) 3 V	–	–	–	–			[51]
Direct fabrication on PI + block copolymer self-assembly	TiW/TiN/ $Ge_2Sb_2Te_5$/ TiW	Si-based p–n diode	20 (@1 V)	(Set) 5.6 V (Reset) 12.8 V	100	104	10	1000	– Low sneak current – Low-power operation	– Lack of interconnection – Inefficient transfer process	[52]

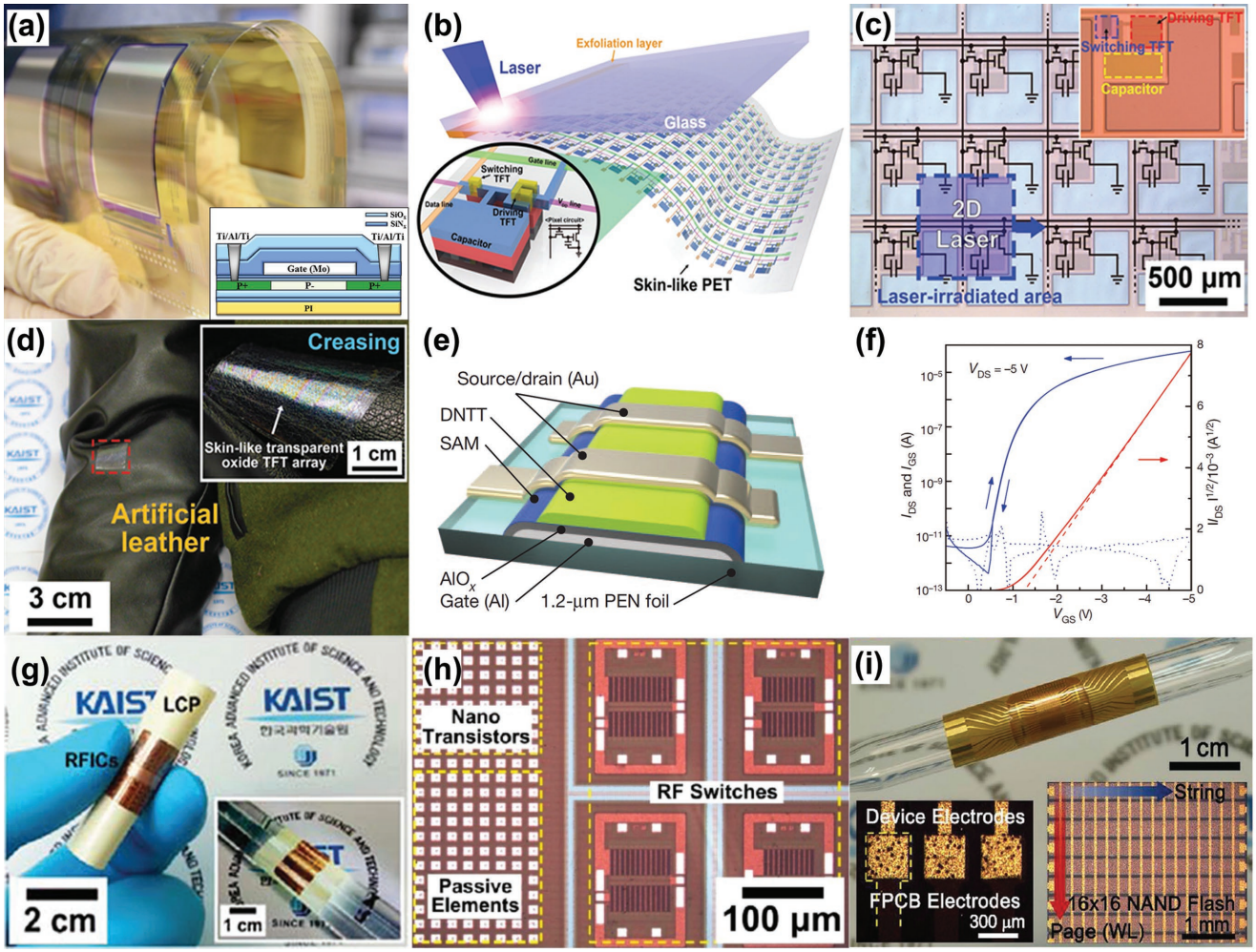

Figure 4. a) Photograph of the flexible TFTs fabricated on plastic substrates through the LTPS process. The inset is a schematic of the cross-section of the devices. b) Schematic of the high-performance, ultrathin oxide TFT arrays fabricated by using the ILLO process for cognitive visual communication. The inset model shows the unit pixel of an active-matrix display panel with a circuit diagram. c) An optical microscopy image of the ultrathin oxide TFT arrays. The inset shows a unit pixel of the devices. d) Photograph of the ultrathin oxide TFT arrays adhered to artificial leather. The inset is a magnified view of the ultrathin oxide TFT arrays on wrinkled cloth. e) Schematic of the ultrathin and imperceptible OFET. f) Transfer curve of the ultrathin OFET device. g) Photograph of the flexible RFICs encapsulated with liquid crystal polymer (LCP) substrates. The inset shows that the flexible RFICs can provide conformal contact on the curved surfaces of three glass pipets. h) Optical image of the flexible RFICs consisting of RF switches, nanotransistors, and passive elements. i) Photograph of the ACF-packaged flexible NAND wrapped on a glass rod. The inset shows the optical image of the electrode area (left), and the active region of the device (right). (a) Reproduced with permission.[132] Copyright 2017, American Chemical Society. (b–d) Reproduced with permission.[8] Copyright 2016, Wiley-VCH. (e, f) Reproduced with permission.[133] Copyright 2013, Springer Nature. (g, h) Reproduced with permission.[69] Copyright 2013, American Chemical Society. (i) Reproduced with permission.[72] Copyright 2016, Wiley-VCH.

dispersed in an elastic resin matrix. Reliable operation of a 16×16 NAND array on a flexible substrate was first established at the circuitry level by successfully programming and reading ASCII code letters, as shown in Figure 5b.

The flexible packaging technology can be extensively applied for all-in-one SoP, enabling the integration of various electronic components such as optoelectronics, energy sources, and sensors on a single plastic.[24,74,145–147] As presented in Figure 5c, flexible AlGaInP vertical light-emitting diodes (LEDs) (size of 50×50 μm^2) were devised through ACF interconnection technology, demonstrating high-performance (optical power density over 25 mW mm^{-2}) LEDs with improved heat dissipation and a short current path. The flexible vertical LEDs (f-VLEDs) with bending stiffness of 2.6×10^{-8} N m and thickness of ≈35 μm showed high flexibility along with mechanical robustness, and exhibited identical electrical properties and optical output under bending at a curvature radius of 2.5 mm. Jeong et al.[71] reported self-powered flexible light-emitting systems via flexible packaging, as shown in Figure 5d. Figure 5e presents an active-matrix (Figure 5f) backplane for a flexible pressure-sensor array. The integrated sensor for an artificial electronic skin (e-skin) could be operated at a low operating voltage (less than 5 V) with excellent mechanical reliability. Wang et al.[11] reported user-interactive flexible electronics at a system level by monolithically integrating various TFTs, a pressure sensor, and a display over large areas on a single plastic substrate, and they can not only sense and spatially map external pressure but also provide a visual response through a full-color display (Figure 5g).

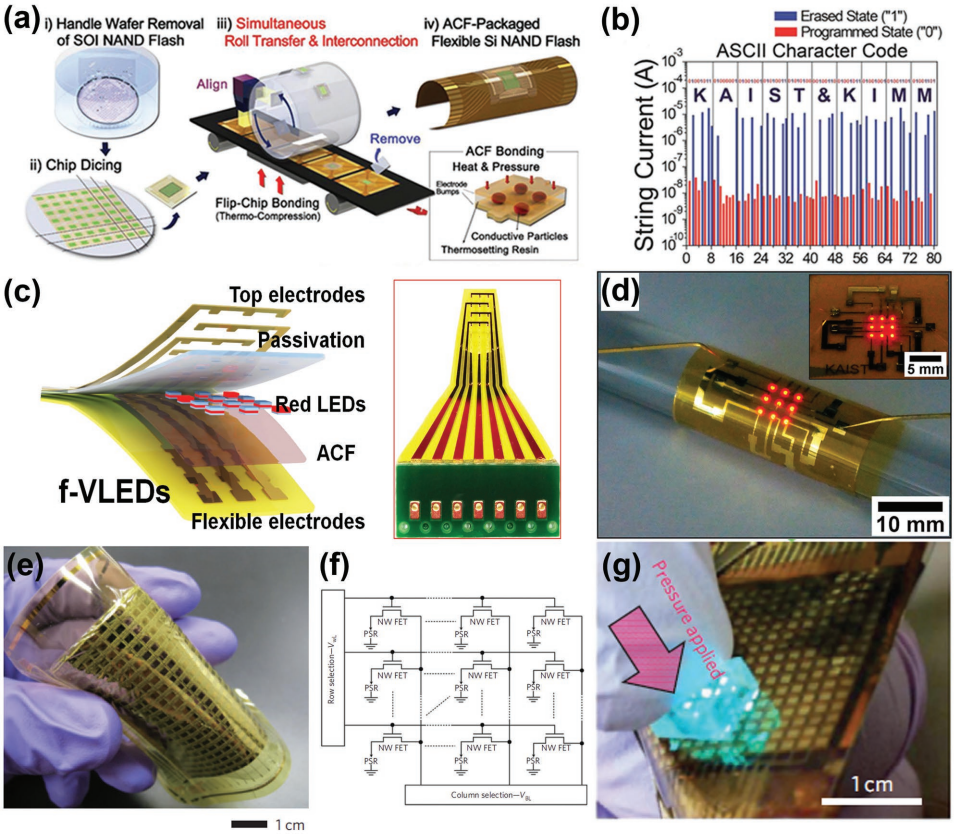

Figure 5. a) Schematic of the Si-based f-NAND flash-memory fabrication by roll-based anisotropic conductive film (ACF) packaging. b) The current histogram of the 16 × 16 flexible NAND array which programs and reads ASCII letters. c) Schematic of the ACF-packaged flexible AlGaInP vertical LEDs (f-VLEDs) (left), and a photograph of the devices (right). d) Photograph of a 3 × 3 array of the f-VLEDs in a bending state on a glass rod. The inset is an image of the f-VLEDs in the flat state. e) Photograph of the nanowire-based active-matrix backplane for a flexible pressure-sensor array. f) Circuit diagram of the nanowire-based active matrix to control each pixel. g) Photograph of the flexible e-skin device with 16 × 16 pixels showing that only the pressed pixels are switched on. (a, b) Reproduced with permission.[72] Copyright 2016, Wiley-VCH. (c) Reproduced with permission.[74] Copyright 2017, Elsevier. (d) Reproduced with permission.[71] Copyright 2014, Royal Society of Chemistry. (e, f) Reproduced with permission.[75] Copyright 2010, Springer Nature. (g) Reproduced with permission.[11] Copyright 2013, Springer Nature.

5. Neuromorphic Computing Devices

Various memristors and synaptic transistors have been recently investigated to demonstrate a human cognitive mechanism (e.g., STDP,[94,96,97] integrate-fire model[148,149]). Wang et al.[150] proposed a serially connected structure of one atomic switch (Au/SiO_xN_y:Ag/Au) and one memristor ($Pt/TaO_x/Ta/Pt$) to emulate a STDP event in a biological synapse, as schematically illustrated in **Figure 6**a. For demonstration of the STDP operation, nonoverlapping pre- and postspikes (negative and positive pulses) with a time interval Δt were applied to the combined element (Figure 6b). As shown in Figure 6c, a short Δt could induce large resistance variation (synaptic weight change) of the memristor due to the volatile nature of the atomic switch. When a presynaptic spike occurred before the postsynaptic spike (potentiation process), the synaptic weight was increased by high oxygen-vacancy concentration generated in the TaO_x layer, whereas depression mode (postsynaptic spike first applied) decreased the synaptic weight of the memristor. As a result, the connection strength between biological neurons that determines the degree of memory loss was successfully emulated by STDP learning operation of the synaptic device.

Tian et al.[151] imitated the biological multisynaptic network between two neurons by black phosphorous (BP)-based single-gated multichannel transistor that exhibit anisotropic drain current (postsynaptic current, PSC) depending on the channel direction (Figure 6d). The pre- (positive pulses) or postsynaptic spikes (negative pulses) applied at the back gate of the BP transistor could control the amount of trapped charges inside the native phosphorous oxide at the BP/SiO_2 interface, modulating the PSC change (ΔPSC) of each BP channel formed along different directions. Figure 6e,f shows STDP behavior of the BP synaptic device, which presents that synaptic weight changes (ΔPSC/PSC) along the y-axis is more prominent compared to the x-axis. Therefore, a single gate pulse train could simultaneously induce discrete ΔPSC/PSC of the transistor for multisynaptic network.

A Ag nanocone-/SiO_2 nanomesh-/Pt-structured conductive bridge memory demonstrated uniform and consistent multilevel cell (MLC) operation that is important for neuromorphic applications (Figure 6g).[90] A well-defined interdigitated hybrid

Table 4. Summary of main parameters in flexible thin-film transistors.

Material	Device configuration	Fabrication process	Gate dielectric	Channel	Mobility [$cm^2 V^{-1} s^{-1}$]	I_{on}/I_{off} ratio (V_{gate}, V_{drain})	V_{th} [V]	Subthreshold swing (SS) [mV dec^{-1}]	Bending radius [mm]	Opportunities	Challenges	Reference
Inorganic-based	2-Transistors (Tr.) (driving and switching Tr.)	Semiconductor process + laser liftoff (LLO)	Al_2O_3	Indium zinc oxide (IZO)	38.5	8×10^7 (@20, 0.1 V)	−0.3	180	7.5	– High transparency – Ultrathin device		[8]
	1-Transistor	Direct fabrication on PI + LTPS[a] process	Si_3N_4/SiO_2	Si	45–65	$>10^6$ (@−4, −0.1 V)	−2 to −1	–	5	– High carrier mobility	– Low-throughput LTPS	[132]
Organic-based	Complementary transistors (n- and p-channel Tr.)	Direct fabrication on PI	AlOx/SAM[b]	(p-channel) Pentacene (n-channel) F_{16}CuPc[c]	(p-channel) 0.5 (n-channel) 0.01	10^7 (Pentacene) (@−3, −1.5 V) 10^5 (F_{16}CuPc) (@2.4, 1.5 V)	−1 to −0.5 (Pentacene) −1 to −0.5 (F_{16}CuPc)	100 (Pentacene) 160 (F_{16}CuPc)	0.1	– High flexibility – Low-voltage operation	– Low carrier mobility	[70]
	1-Transistor	Direct fabrication on polyethylene naphthalate (PEN)	AlOx/SAM[b]	DNTT[d]	2.52	$>2 \times 10^7$ (@3, 3 V)	−0.66	83	0.005	– High flexibility – High stretchability	– Low carrier mobility	[133]

[a]LTPS: low-temperature polysilicon; [b]SAM: phosphonic-acid self-assembled monolayer; [c]F_{16}CuPc: hexadecafluorocopperphthalocyanine; [d]DNTT: dinaphtho[2,3-*b*:2′,3′-*f*]thieno[3,2-*b*]thiophene.

Table 5. Summary of main parameters in devices for neuromorphic computing.

Device type	Device structure	Flexibility	Energy consumption	Operation speed	Maximum I_{on}/I_{off} ratio	Endurance [switching #]	Gradual SW[a] change	Opportunities	Challenges	Reference
Memristor	Ag/SiO_2/Pt	X	<2.8 pJ	70 ns	103	140	X	– Power efficiency – Device uniformity – Multilevel resistance	– Lack of interconnection	[90]
Atomic switch + memristor	Au/Ag:SiO_xN_y/Au + Pt/TaO_x/Ta/Pt	X	–	(Atomic switch) 200 µs (Memristor) 300 ns	(Atomic switch) 10^{10} (Memristor) $<10^2$	(Atomic switch) 10^6	O	– Analogous SW change – Low sneak current	– Lack of interconnection	[150]
BP[b]-based synaptic Tr.	BP channel/SiO_2/Si back gate	X	–	10 ms	–	–	O	– Multisynaptic operation – Gradual PSC[c] change	– Low-speed operation	[151]
Memristor	Ag/MoO_x/MoS_2/Ag	O	<3 mJ	10 s	106	104	X	– Multilevel resistance	– Power inefficiency – Low-speed operation	[154]
Memristor	Al/pMSSQ[d]:Cu/Al	O	<60 pJ	30 µs to 0.4 ms	<200	–	O	– Power efficiency – Scalable device structure – Low sneak current	– Low I_{on}/I_{off} ratio	[155]
n-channel Tr. and p-channel Tr.	CNT channel/SiO_x/Au/SiO_x/Pd back gate	O	–	5 ms	$<10^5$	–	O	– Cost-effective process	– Power inefficiency – Low-speed operation	[118]

[a]SW: synaptic weight; [b]BP: black phosphorous; [c]PSC: postsynaptic current; [d]pMSSQ: poly(methylsilsesquioxane).

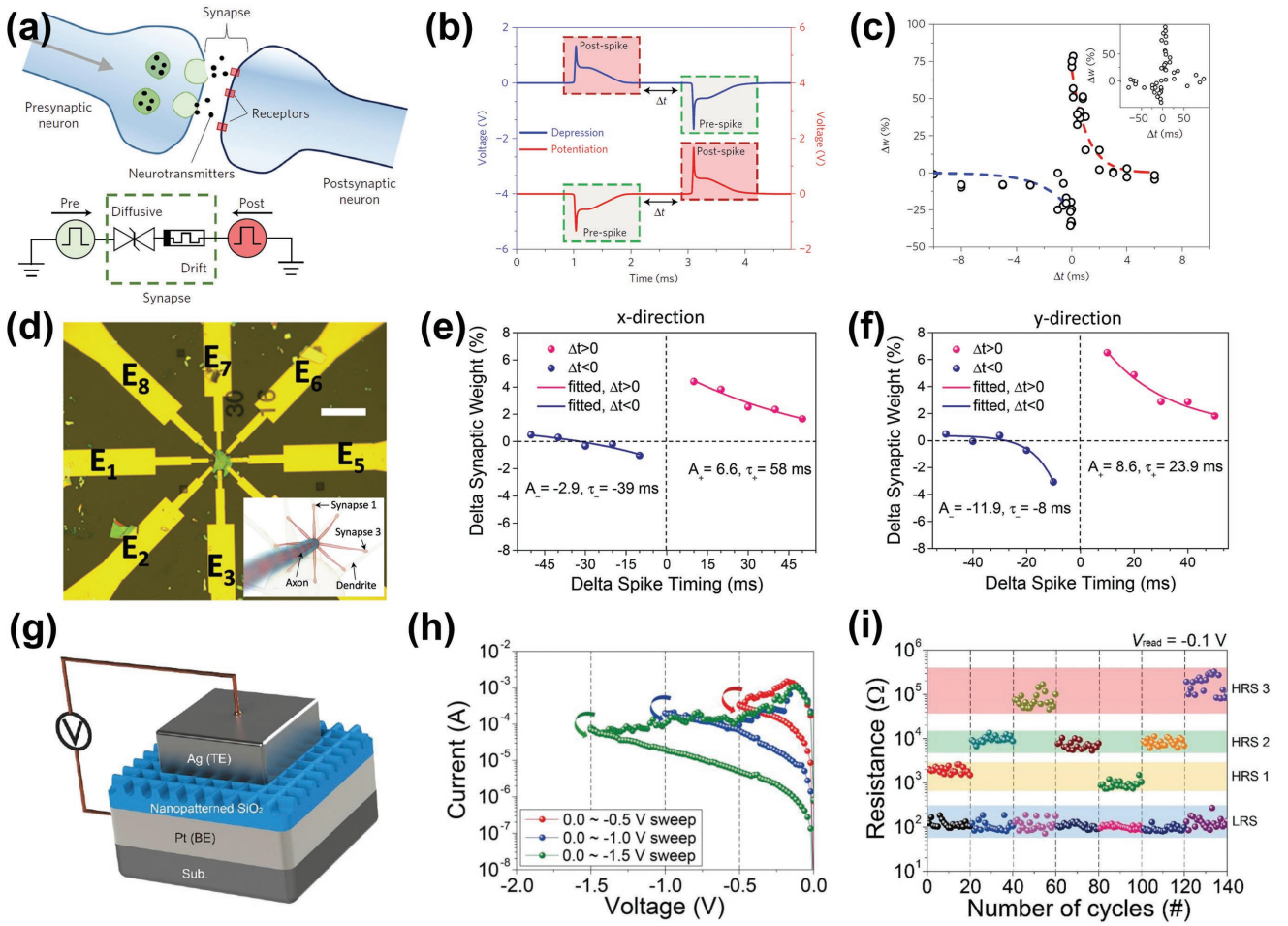

Figure 6. a) Schematic of a synaptic junction between the pre- and postsynaptic neurons, and a circuit diagram of the electronic synapse composed of the SiO_xN_y:Ag atomic switch connected with the TaO_x drift memristor and between pulsed voltage sources. b) The pre- and postsynaptic spike pulses applied to the device for spike-timing-dependent plasticity (STDP) imitation (depression: blue, potentiation: red). c) Plot of the resistance (synaptic weight) change of the memristor with changes in Δt. d) Optical image and schematic (inset) of the multisynaptic network based on a black phosphorous (BP) transistor. e,f) STDP behavior of the BP synaptic device along the *x*-axis and the *y*-axis, respectively. g) Schematic of the Ag nanocone/SiO_2 nanomesh/Pt memristive device. h) *I*–*V* characteristic for multilevel cell (MLC) operations of the Ag nanocone/SiO_2 nanomesh/Pt memristor at the reset process region. i) MLC cycling endurance test of the Ag nanocone/SiO_2 nanomesh/Pt memristor cell under four different memory states. (a–c) Reproduced with permission.[150] Copyright 2016, Springer Nature. (d–f) Reproduced with permission.[151] Copyright 2016, Wiley-VCH. (g–i) Reproduced with permission.[90] Copyright 2016, American Chemical Society.

architecture comprising a SiO_2 nanomesh (sub-10 nm) and Ag nanocones could selectively guide the positions of Ag nanofilaments in a memristor by inducing a highly concentrated electric field between the SiO_2 and the Ag nanocone tip end, enabling stable MLC applications with four discrete levels without any overlap (Figure 6h). The MLC cycling endurance test additionally confirmed the four memory states in either the reverse or forward voltage sweeping direction, as presented in Figure 6i.

The field of neuromorphic electronics is about to embrace radical innovations through the convergence with the technologies of SoP, which can realize hyperintelligent society by providing human-like understanding capability to flexible electronics.[99,152,153] Furthermore, numerous attempts have been made to demonstrate the highly scalable synaptic array on plastic beyond a single element level for practical neuromorphic computations that are similar to our human brain. Bessonov et al.[154] reported a novel memristive array on plastic composed of a MoO_x/MoS_2 active material, and printed Ag top electrode (TE) and bottom electrode (BE) to mimic the short-term potentiation (STP) and long-term potentiation (LTP) learning mechanisms of the biological synapse (**Figure 7**a). As shown in Figure 7b, the Ag/AgNW/MoO_x/MoS_2/Ag system did not sustain a gain current level and drastically returned to its original off state because of its fast oxygen vacancy migration (inside MoO_x) and charge trapping (at the Ag/MoO_x interface) characteristics when electric pulses with a low repetition rate (6 s) were applied (STP). On the other hand, a nonlinear switching dynamics and NVM property of LTP could be induced by repeated stimulation (short repetition intervals of 0.6 s, for 25 s), as shown in Figure 7c. Kim et al.[118] suggested hierarchical pattern recognition scheme based on an array of flexible inverters and synaptic transistors (artificial synapse). For image

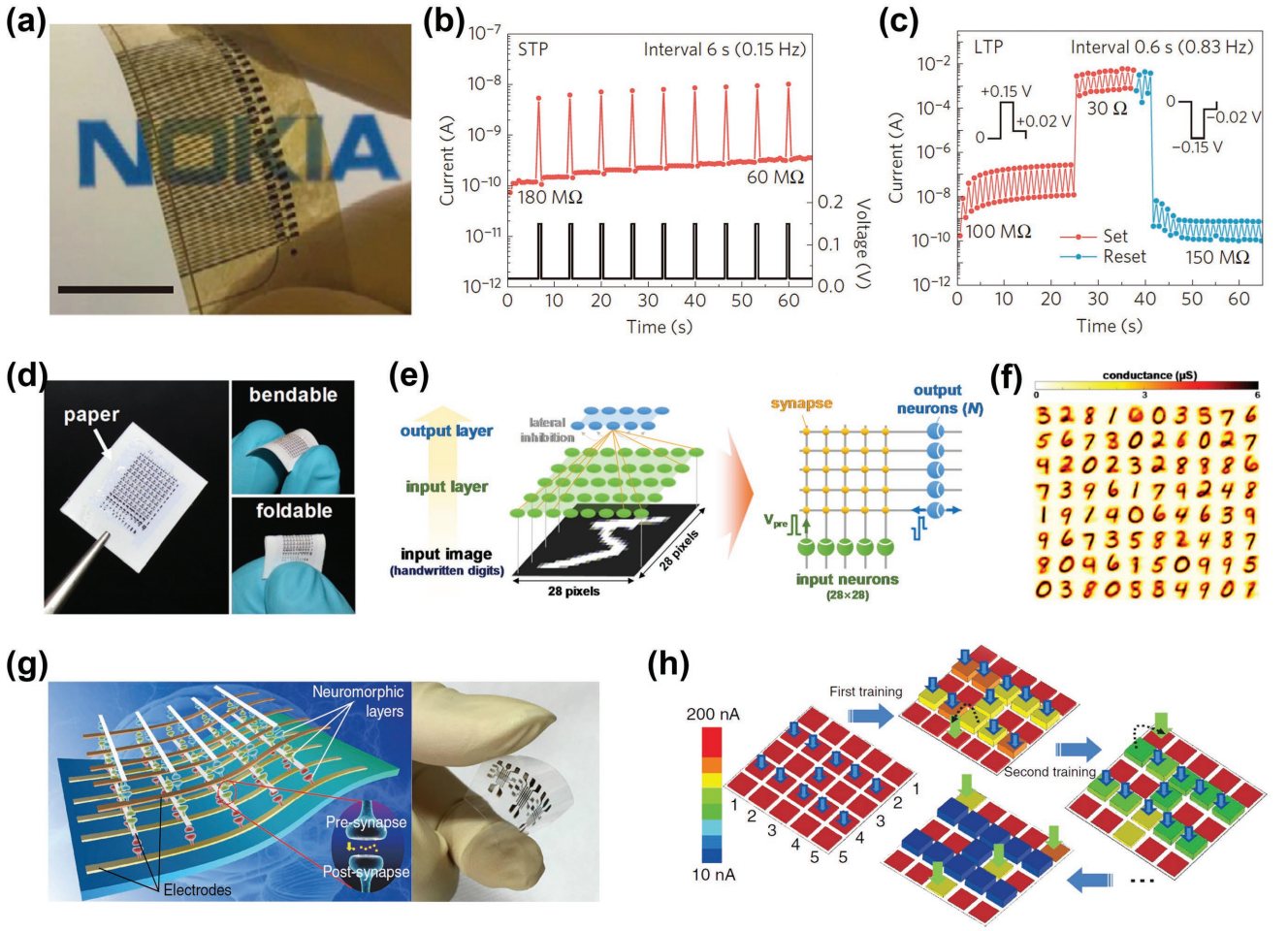

Figure 7. a) Photograph of the MoO_x/MoS_2 memristive devices with Ag conductors for the emulation of STP and LTP processes in the biological synapse. b) Resistive switching of the Ag/AgNW/MoO_x/MoS_2/Ag device with electrical pulses having a long repetition interval of 6 s. c) Resistive switching of the Ag/AgNW/MoO_x/MoS_2/Ag memristive device with electrical pulses having a short repetition interval of 0.6 s. d) Photograph of the flexible synaptic transistors on the paper substrate. e) Schematic of the neural network for pattern recognition consisting of 28 × 28 synaptic transistors between the input and the output neurons. f) Pattern recognition through the conductance change of the synaptic devices which connect the input neurons to the output neurons individually. g) Schematic and photograph of the flexible 3D memristor array fabricated by using Cu-doped pMSSQ. h) The overall programming process of the flexible memristors to memorize the image. (a–c) Reproduced with permission.[154] Copyright 2014, Springer Nature. (d–f) Reproduced with permission.[118] Copyright 2017, American Chemical Society. (g, h) Reproduced with permission.[155] Copyright 2017, Springer Nature.

identifying simulation as shown in Figure 7e, hypothetic 28 × 28 synaptic transistors were parallelly connected with the leaky integrator circuits to control the degree of channel conductance (synaptic weight) change in the synaptic transistor, enabling the highly accurate recognition of 10 different digits from the modified national institute of standards and technology (MNIST) database (Figure 7f). Wu et al.[155] proposed a flexible 3D memristor array based on a Cu-doped poly(methylsilsesquioxane) (pMSSQ) material to demonstrate artificial neural network, successfully mimicking correlated learning behavior and trainable memory function of biological synapses. As shown in Figure 7g, triple layers of crossbar-structured memristor array are vertically stacked on plastic substrate to independently operate discrete neuromorphic functions of the three memristor array. To emulate cognition process of human brain, repeated image training pulses (15 times) were applied to the desired (blue arrow) and undesired memristors (green arrow), as indicated in Figure 7h. The trained memristors successfully programmed the letter "H" by changing their conductance (synaptic weight) gradually during each training session despite the intentional incorrect inputs. Other memristor layers also could be independently operated after same procedures, showing significant potential for realizing new physical platform for hierarchical network applications such as visual and auditory process systems. **Table 5** presents the performance and challenge of the neuromorphic devices in section 5.

6. Potential Research Fields of Flexible Neuromorphic Applications

6.1. Wearable Electronics

Wearable electronics have attracted a great deal of attention as one of the promising research areas for the flexible neuromorphic applications.[156,157] Recently, Son et al.[158] reported wearable memory modules, capacitors, and logic gates

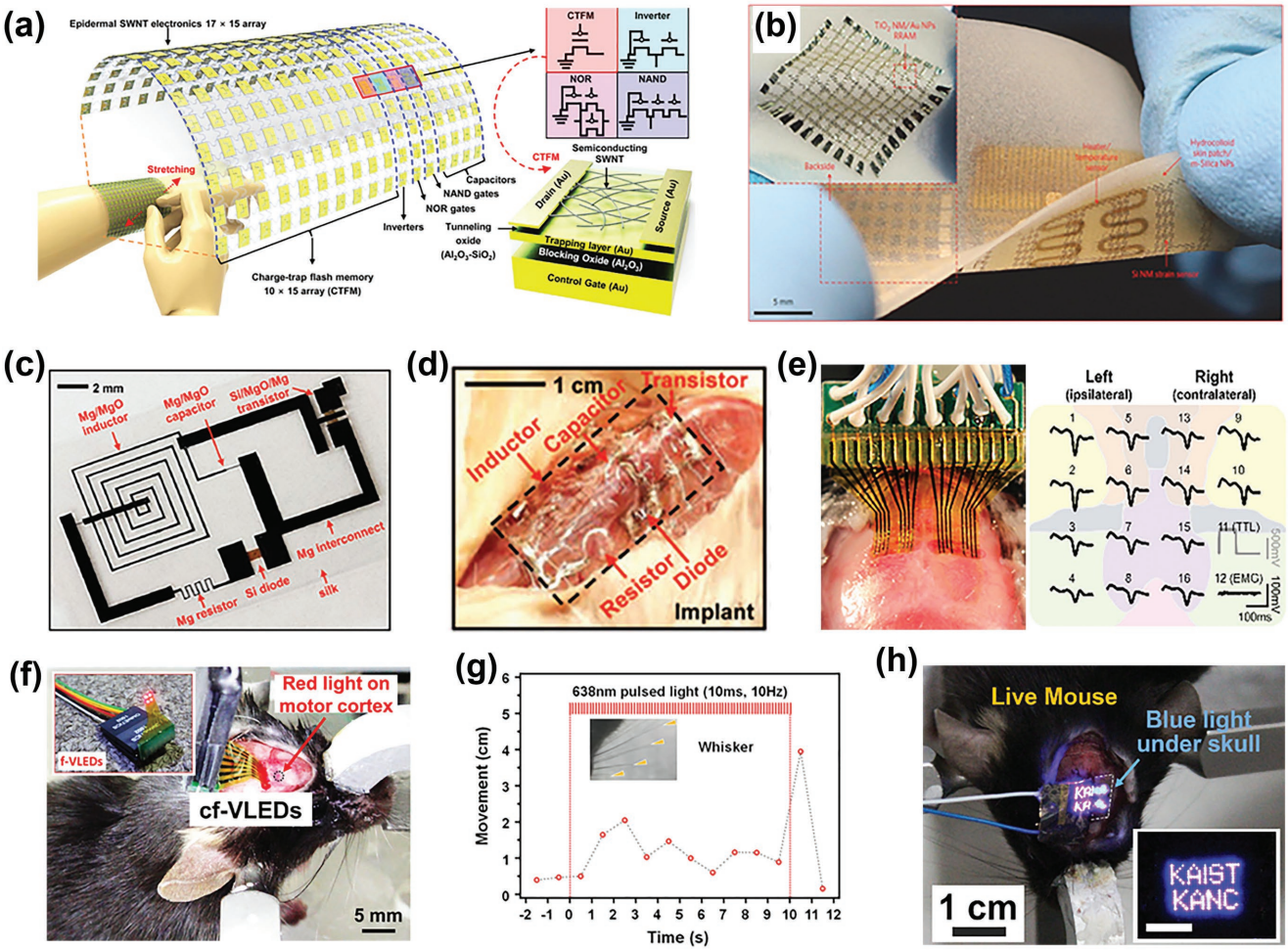

Figure 8. a) Schematic of the semiconducting single-walled CNT (s-SWNT)-based wearable electronic system consisting of charge-trap floating gate memory (CTFM) devices, logic gates (NAND/NOR gates) and inverters, and capacitors (left). Circuit diagram of the s-SWNT-based wearable electronic devices (top right). Schematic of layered components of the CTFM (bottom right). b) Photograph of the wearable bioelectronic system consisting of a TiO_2-based RRAM array, single-crystal Si-based strain sensors, and electroresistive heaters. The inset shows a 10×10 array of TiO_2 RRAM devices on the wearable patch. c) Photograph of the implantable electronic device, and its components. d) Photograph of the implantable electronic device inserted in the subdermal dorsal region of a BALB/c mouse. e) Photograph of the iWEBS inserted under the skull (left), and the artificially induced spike-and-wave discharge (SWD)-like spikes (absence seizure indicator) in the mouse cortical subdomains measured by the iWEBS (right). f) Photograph of the AlGaInP f-VLED array inserted into the meningeal space under the mouse skull. The inset shows red light illumination of the f-VLEDs. g) Record of the whisker movement during the f-VLED illumination. Yellow triangles indicate the mouse whiskers. h) Blue-light illumination of the GaN f-VLED array inserted under the mouse skull. The inset shows the 30×30 array of GaN f-VLEDs. (a) Reproduced with permission.[158] Copyright 2015, American Chemical Society. (b) Reproduced with permission.[26] Copyright 2014, Springer Nature. (c, d) Reproduced with permission.[169] Copyright 2012, AAAS. (e) Reproduced with permission.[25] Copyright 2016, American Chemical Society. (f, g) Reproduced with permission.[74] Copyright 2017, Elsevier. (h) Reproduced with permission.[170] Copyright 2018, Wiley-VCH.

for advanced electronic circuit/systems, as schematically illustrated in **Figure 8**a. An ultrathin (<≈3 μm) island array system enables conformal integration of electronics on the human skin, fulfilling not only mechanical reliability but also performance requirements. Kim and co-workers[26] demonstrated wearable sensor systems with functionality of diagnosis, data storage, and controlled therapeutic treatment by integrating a TiO_2-based RRAM array, strain sensors, and electroresistive heaters (Figure 8b). Because of the ultrathin feature of the electronics, it could be conformally contacted with the skin, exhibiting stable electrical operation under repeated tension and compression stresses caused by a human wrist. Those wearable electronics are expected to be merged with the neuromorphic technologies, enabling the individual big data systems such as chemical fallout alert, and air pollution monitoring.[159]

6.2. Biomedical and Brain Applications

Modern technological progress in SoP enables biological integration of flexible electronics (e.g., sensors, drug delivery devices, and optoelectronics) at the precise location of the human organs or brain with minimally invasive strategies, which has significant potential to be converged to neuromorphic system.[25,114,145,147,160–168] As shown in Figure 8c,d, Hwang et al.[169] demonstrated implantable electronic components

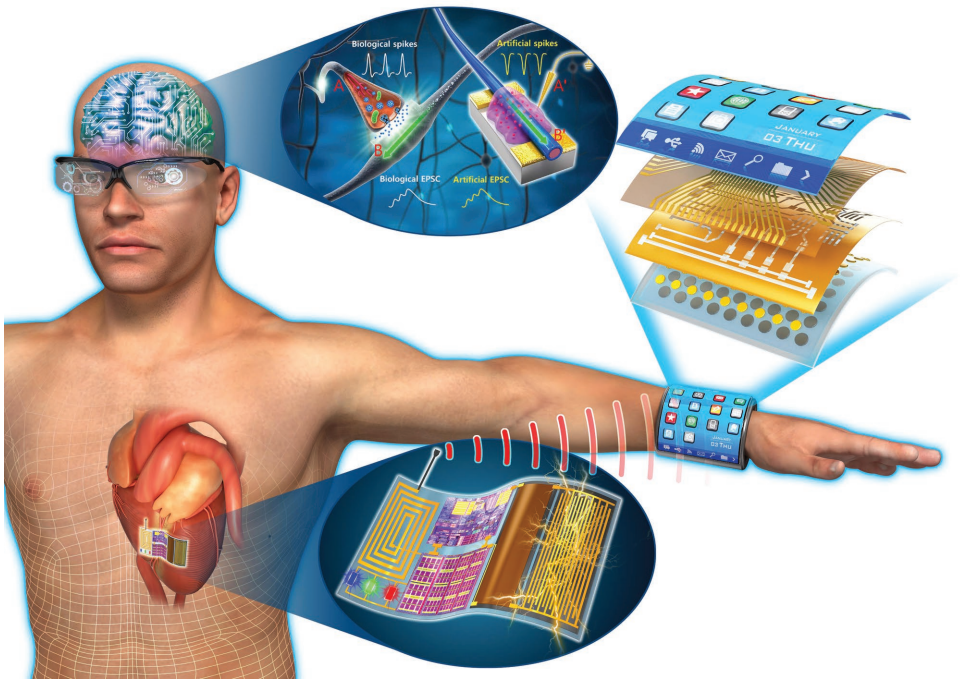

Figure 9. Schematic of future neuromorphic SoP consisting of wearable and biomedical applications, and flexible synaptic device system. Bottom-center image (heart with flexible electronic system): Adapted with permission.[179] Copyright 2015, Elsevier. Top-center image (synaptic device): Adapted with permission.[181] Copyright 2016, AAAS.

such as capacitors, inductors, resistors, and diodes for integrated sensors (e.g., temperature or strain), actuators, photodetectors, and solar cells. Lee and co-workers[25] reported the insertable wrapping electrode array beneath the skull (iWEBS) biosystem for pathological and physiological optogenetic mappings of functional connectivity among cortices across a wide surface in a freely moving mice (Figure 8e, left side). As shown in the right illustration of Figure 8e, dynamic changes of cortical activity were precisely measured during physiological and drug-activated epileptic states. Beyond the spatiotemporal mapping technology of neural interactions, an optogenetic tool for precisely controlling the body movements was realized. A densely arranged AlGaInP f-VLED array was inserted into the meningeal space on each hemisphere, successfully wrapping the motor cortical regions in a less invasive manner for multispot photoexcitation of the frontal motor neurons (Figure 8f). When the f-VLEDs were illuminated, distinct movements of the whiskers and electromyogram (EMG) signal changes were observed, as shown in Figure 8g. Flexible blue LED light sources were further developed for optogenetic recording and/or stimulation. As presented in Figure 8h, a flexible GaN VLED array (30×30) demonstrated by a simple monolithic fabrication was smoothly inserted under a living mouse skull via a cranial slit for functional optical irradiation to the neuron cortex.[170] We strongly believe that a new form of artificial synaptic devices will be developed through a convergence between the research fields of the bioelectronics and flexible neuromorphic systems. Such device systems can be directly connected to humans' subdermal tissue, providing excellent capabilities of fast mapping and analyzing of physiological signals based on an unprecedented bio–machine interface.[25,162,171–173]

6.3. Representative Examples of the Future Flexible Neuromorphic System

Figure 9 illustrates future technological design of neuromorphic SoP. Implanted sensors can continuously collect many kinds of complex biosignals (e.g., pulse, body temperature, hormone, pH), which offer critical information regarding injury and somatic dysfunction of cells, tissues, and organs.[24,174] In addition, various environmental information (e.g., sound, light, air pollution, network availability) can be provided to the user by simply wearing the device.[175–178] On the basis of the compiled big data, wearable neuromorphic system produces the optimal solution. For example, the synaptic devices on plastic can quickly perceive and categorize the patient's particular disease modes based on the pattern of stored biological data.[179,180] Then, the flexible AI systems automatically judge by themselves to send the patient's biological state to the specific medical team that can provide accurate diagnosis through the user's flexible transparent display of eyeglasses.[181–183] Finally, corresponding feedback therapy (e.g., first aid, drug delivery) will be involuntarily proceeded by the wearable therapeutic devices.[13,184]

7. Summary and Outlook

Numerous research efforts to demonstrate high-performance devices beyond the thermal limit of plastics have yielded broad technological advances in the fields of memory, LSI, electronic SoP, and synaptic devices, leading to a new concept of electronics for flexible and neuromorphic computing that can

bring an intelligent breakthrough to diverse areas ranging from wearable AI systems to personalized healthcare. Representative examples of flexible NVM (RRAM, PCM), TFTs, ICs, fully functional SoPs, and synaptic devices, and their potential applications described in this report suggest the future flexible and neuromorphic technology. At the front-end device level, flexible memories, TFTs, and LSIs were realized using various materials (inorganics, GST, and organics) and strategies (printing, ILLO, nanoimprinting, and chemical etching). For system level demonstration, integration of high-performance flexible electronics on a single plastic substrate was accomplished by advanced interconnection and packaging technology for multifunctional SoP. The fields of wearable and biomedical applications were introduced as one of the promising research that can be merged with flexible neuromorphic systems, showing significant potential for shifting the conventional paradigm of Si very-large-scale integration (VLSI) electronics.

Acknowledgements

H.E.L., J.H.P., and T.J.K. contributed equally to this work. This work was supported by the Wearable Platform Materials Technology Center (WMC) (Grant No. NRF-2016R1A5A1009926), the Nano-Material Technology Development Program (Grant No. NRF-2016M3A7B4910636) through the National Research Foundation of Korea (NRF) funded by the Ministry of Science, ICT and Future Planning. This work was supported by the National Research Foundation (NRF) of Korea funded by the Ministry of Science, ICT and Future Planning (Grant Nos. NRF-2014R1A2A1A12067558 and 2012-0008779).

Conflict of Interest

The authors declare no conflict of interest.

Keywords

biomedical applications, flexible electronics, interconnection, large-scale integration, neuromorphic computing, wearable

Received: March 7, 2018
Revised: April 17, 2018
Published online: July 4, 2018

[1] H. Klauk, *Nat. Mater.* **2007**, *6*, 397.
[2] J. S. Chang, A. F. Facchetti, R. Reuss, *IEEE J. Emerging Sel. Top. Circuits Syst.* **2017**, *7*, 1.
[3] M. Koo, K. Il Park, S. H. Lee, M. Suh, D. Y. Jeon, J. W. Choi, K. Kang, K. J. Lee, *Nano Lett.* **2012**, *12*, 4810.
[4] T. Hsu, K. Yu, Y. Lai, W. Wang, Y. Lin, *SID Symp. Dig. Tech. Pap.* **2017**, *48*, 1785.
[5] Y. Zhan, Y. Mei, L. Zheng, *J. Mater. Chem. C* **2014**, *2*, 1220.
[6] H. Ushijima, Y. Kusaka, M. Fujita, K. Nomura, S. Kanazawa, Y. Horii, K. Abe, N. Yamamoto, presented at *2017 Int. Conf. on Electronics Packaging (ICEP)*, IEEE, Yamagata, Japan **2017**.
[7] U. Gupta, S. Jain, U. Y. Ogras, presented at *2015 28th IEEE Int. System-on-Chip Conf. (SOCC)*, IEEE, Beijing, China **2015**.
[8] H. E. Lee, S. Kim, J. Ko, H. I. Yeom, C.-W. Byun, S. H. Lee, D. J. Joe, T. H. Im, S.-H. K. Park, K. J. Lee, *Adv. Funct. Mater.* **2016**, *26*, 6170.
[9] Y. S. Choi, J. U. Yun, S. E. Park, *J. Non-Cryst. Solids* **2016**, *431*, 2.
[10] R.-H. Kim, D.-H. Kim, J. Xiao, B. H. Kim, S.-I. Park, B. Panilaitis, R. Ghaffari, J. Yao, M. Li, Z. Liu, V. Malyarchuk, D. G. Kim, A.-P. Le, R. G. Nuzzo, D. L. Kaplan, F. G. Omenetto, Y. Huang, Z. Kang, J. A. Rogers, *Nat. Mater.* **2010**, *9*, 929.
[11] C. Wang, D. Hwang, Z. Yu, K. Takei, J. Park, T. Chen, B. Ma, A. Javey, *Nat. Mater.* **2013**, *12*, 899.
[12] R. Tajima, T. Miwa, T. Oguni, A. Hitotsuyanagi, H. Miyake, H. Katagiri, Y. Goto, Y. Saito, J. Goto, M. Kaneyasu, M. Hiroki, M. Takahashi, S. Yamazaki, *J. Soc. Inf. Disp.* **2014**, *22*, 237.
[13] K. Takei, W. Honda, S. Harada, T. Arie, S. Akita, *Adv. Healthcare Mater.* **2015**, *4*, 487.
[14] W. Kim, S. Kwon, Y. C. Han, E. Kim, K. C. Choi, S.-H. Kang, B.-C. Park, *Adv. Electron. Mater.* **2016**, *2*, 1600220.
[15] S.-I. Park, Y. Xiong, R.-H. Kim, P. Elvikis, M. Meitl, D.-H. Kim, J. Wu, J. Yoon, C.-J. Yu, Z. Liu, Y. Huang, K.-C. Hwang, P. Ferreira, L. Xiuling, K. Choquette, J. A. Rogers, *Science* **2009**, *325*, 977.
[16] M. C. McAlpine, R. S. Friedman, S. Jin, K.-H. Lin, W. U. Wang, C. M. Lieber, *Nano Lett.* **2003**, *3*, 1531.
[17] S. Choi, S. Kwon, H. Kim, W. Kim, J. H. Kwon, M. S. Lim, H. S. Lee, K. C. Choi, *Sci. Rep.* **2017**, *7*, 6424.
[18] Y. Chen, J. Au, P. Kazlas, A. Ritenour, H. Gates, M. McCreary, *Nature* **2003**, *423*, 136.
[19] G. H. Gelinck, H. E. A. Huitema, E. van Veenendaal, E. Cantatore, L. Schrijnemakers, J. van der Putten, T. C. T. Geuns, M. Beenhakkers, J. B. Giesbers, B. H. Huisman, E. J. Meijer, E. M. Benito, F. J. Touwslager, A. W. Marsman, B. J. E. van Rens, D. M. de Leeuw, *Nat. Mater.* **2004**, *3*, 106.
[20] J. Liang, L. Li, X. Niu, Z. Yu, Q. Pei, *Nat. Photonics* **2013**, *7*, 817.
[21] H. Lee, C. Song, Y. S. Hong, M. S. Kim, H. R. Cho, T. Kang, K. Shin, S. H. Choi, T. Hyeon, D.-H. Kim, *Sci. Adv.* **2017**, *3*, e1601314.
[22] Y. Wang, L. Wang, T. Yang, X. Li, X. Zang, M. Zhu, K. Wang, D. Wu, H. Zhu, *Adv. Funct. Mater.* **2014**, *24*, 4666.
[23] S. Xu, Y. Zhang, L. Jia, K. E. Mathewson, K.-I. Jang, J. Kim, H. Fu, X. Huang, P. Chava, R. Wang, S. Bhole, L. Wang, Y. J. Na, Y. Guan, M. Flavin, Z. Han, Y. Huang, J. A. Rogers, *Science* **2014**, *344*, 70.
[24] D. Y. Park, D. J. Joe, D. H. Kim, H. Park, J.-H. Han, C. K. Jeong, H. Park, J. G. Park, B. Joung, K. J. Lee, *Adv. Mater.* **2017**, *29*, 1702308.
[25] A. H. Park, S. H. Lee, C. Lee, J. Kim, H. E. Lee, S.-B. Paik, K. J. Lee, D. Kim, *ACS Nano* **2016**, *10*, 2791.
[26] D. Son, J. Lee, S. Qiao, R. Ghaffari, J. Kim, J. E. Lee, C. Song, S. J. Kim, D. J. Lee, S. W. Jun, S. Yang, M. Park, J. Shin, K. Do, M. Lee, K. Kang, C. S. Hwang, N. Lu, T. Hyeon, D.-H. Kim, *Nat. Nanotechnol.* **2014**, *9*, 397.
[27] J. Kim, P. Gutruf, A. M. Chiarelli, S. Y. Heo, K. Cho, Z. Xie, A. Banks, S. Han, K. I. Jang, J. W. Lee, K. T. Lee, X. Feng, Y. Huang, M. Fabiani, G. Gratton, U. Paik, J. A. Rogers, *Adv. Funct. Mater.* **2017**, *27*, 1604373.
[28] W. Gao, S. Emaminejad, H. Y. Y. Nyein, S. Challa, K. Chen, A. Peck, H. M. Fahad, H. Ota, H. Shiraki, D. Kiriya, D.-H. Lien, G. A. Brooks, R. W. Davis, A. Javey, *Nature* **2016**, *529*, 509.
[29] G. Schwartz, B. C.-K. Tee, J. Mei, A. L. Appleton, D. H. Kim, H. Wang, Z. Bao, *Nat. Commun.* **2013**, *4*, 1859.
[30] C. Dagdeviren, Y. Su, P. Joe, R. Yona, Y. Liu, Y.-S. Kim, Y. Huang, A. R. Damadoran, J. Xia, L. W. Martin, Y. Huang, J. A. Rogers, *Nat. Commun.* **2014**, *5*, 4496.
[31] C. M. Lochner, Y. Khan, A. Pierre, A. C. Arias, *Nat. Commun.* **2014**, *5*, 5745.
[32] D. Librenza-Garcia, B. J. Kotzian, J. Yang, B. Mwangi, B. Cao, L. N. Pereira Lima, M. B. Bermudez, M. V. Boeira, F. Kapczinski, I. C. Passos, *Neurosci. Biobehav. Rev.* **2017**, *80*, 538.
[33] R. C. Kessler, H. M. Van Loo, K. J. Wardenaar, R. M. Bossarte, L. A. Brenner, T. Cai, D. D. Ebert, I. Hwang, J. Li, P. De Jonge, A. A. Nierenberg, M. V. Petukhova, A. J. Rosellini, N. A. Sampson,

R. A. Schoevers, M. A. Wilcox, A. M. Zaslavsky, *Mol. Psychiatry* **2016**, *21*, 1366.
[34] M. Mozaffari-Kermani, S. Sur-Kolay, A. Raghunathan, N. K. Jha, *IEEE J. Biomed. Health Inf.* **2015**, *19*, 1893.
[35] D. Ichikawa, T. Saito, W. Ujita, H. Oyama, *J. Biomed. Inf.* **2016**, *64*, 20.
[36] A. Torkamani, K. G. Andersen, S. R. Steinhubl, E. J. Topol, *Cell* **2017**, *170*, 828.
[37] M. Chen, Y. Hao, K. Hwang, L. Wang, L. Wang, *IEEE Access* **2017**, *5*, 8869.
[38] J. S. Rumsfeld, K. E. Joynt, T. M. Maddox, *Nat. Rev. Cardiol.* **2016**, *13*, 350.
[39] W. Raghupathi, V. Raghupathi, *Health Inf. Sci. Syst.* **2014**, *2*, 3.
[40] A. Jan, H. Meng, Y. F. A. Gaus, F. Zhang, *IEEE Trans. Cognit. Dev. Syst.* **2017**, *8920*, 1.
[41] Y. Yuan, G. Giri, A. L. Ayzner, A. P. Zoombelt, S. C. B. Mannsfeld, J. Chen, D. Nordlund, M. F. Toney, J. Huang, Z. Bao, *Nat. Commun.* **2014**, *5*, 1.
[42] K. Nomura, T. Aoki, K. Nakamura, T. Kamiya, T. Nakanishi, T. Hasegawa, M. Kimura, T. Kawase, M. Hirano, H. Hosono, *Appl. Phys. Lett.* **2010**, *96*, 263509.
[43] K. Myny, *Nat. Electron.* **2018**, *1*, 30.
[44] K. Nomura, H. Ohta, A. Takagi, T. Kamiya, M. Hirano, H. Hosono, *Nature* **2004**, *432*, 488.
[45] J. H. Park, S. Han, D. Kim, B. K. You, D. J. Joe, S. Hong, J. Seo, J. Kwon, C. K. Jeong, H.-J. Park, T. S. Kim, S. H. Ko, K. J. Lee, *Adv. Funct. Mater.* **2017**, *27*, 1701138.
[46] Q. Cao, H. Kim, N. Pimparkar, J. P. Kulkarni, C. Wang, M. Shim, K. Roy, M. A. Alam, J. A. Rogers, *Nature* **2008**, *454*, 495.
[47] L. Cai, S. Zhang, J. Miao, Z. Yu, C. Wang, *Adv. Funct. Mater.* **2015**, *25*, 5698.
[48] S. J. Kim, J.-S. Lee, *Nano Lett.* **2010**, *10*, 2884.
[49] G. Wang, A.-R. O. Raji, J.-H. Lee, J. M. Tour, *ACS Nano* **2014**, *8*, 1410.
[50] S. Kim, H. Y. Jeong, S. K. Kim, S.-Y. Choi, K. J. Lee, *Nano Lett.* **2011**, *11*, 5438.
[51] S. H. Hong, J.-H. Jeong, K.-I. Kim, H. Lee, *Microelectron. Eng.* **2011**, *88*, 2013.
[52] B. H. Mun, B. K. You, S. R. Yang, H. G. Yoo, J. M. Kim, W. I. Park, Y. Yin, M. Byun, Y. S. Jung, K. J. Lee, *ACS Nano* **2015**, *9*, 4120.
[53] S. H. Hong, B. J. Bae, H. Lee, J. H. Jeong, *Microelectron. Eng.* **2010**, *87*, 2081.
[54] R. Bez, presented at *Technical Digest - Int. Electron Devices Meeting, IEDM*, IEEE, Baltimore, MD, USA **2009**.
[55] S.-J. Kim, H. Lee, S. H. Hong, *Solid-State Electron.* **2018**, *142*, 56.
[56] Z. Q. Wang, H. Y. Xu, X. H. Li, X. T. Zhang, Y. X. Liu, Y. C. Liu, *IEEE Electron Device Lett.* **2011**, *32*, 1442.
[57] Y. Ji, Y. Yang, S.-K. Lee, G. Ruan, T.-W. Kim, H. Fei, S.-H. Lee, D.-Y. Kim, J. Yoon, J. M. Tour, *ACS Nano* **2016**, *10*, 7598.
[58] A. Jo, Y. Seo, M. Ko, C. Kim, H. Kim, S. Nam, H. Choi, C. S. Hwang, M. J. Lee, *Adv. Funct. Mater.* **2017**, *27*, 1605593.
[59] Y. C. Lai, Y. X. Wang, Y.-C. Huang, T. Y. Lin, Y.-P. Hsieh, Y. J. Yang, Y. F. Chen, *Adv. Funct. Mater.* **2014**, *24*, 1430.
[60] J. Yao, J. Lin, Y. Dai, G. Ruan, Z. Yan, L. Li, L. Zhong, D. Natelson, J. M. Tour, *Nat. Commun.* **2012**, *3*, 1101.
[61] B. C. Jang, H. Seong, S. K. Kim, J. Y. Kim, B. J. Koo, J. Choi, S. Y. Yang, S. G. Im, S. Y. Choi, *ACS Appl. Mater. Interfaces* **2016**, *8*, 12951.
[62] S. K. Hwang, J. M. Lee, S. Kim, J. S. Park, H. I. Park, C. W. Ahn, K. J. Lee, T. Lee, S. O. Kim, *Nano Lett.* **2012**, *12*, 2217.
[63] Y. Ji, D. F. Zeigler, D. S. Lee, H. Choi, A. K.-Y. Jen, H. C. Ko, T.-W. Kim, *Nat. Commun.* **2013**, *4*, 1.
[64] K. Qian, R. Y. Tay, M.-F. Lin, J. Chen, H. Li, J. Lin, J. Wang, G. Cai, V. C. Nguyen, E. H. T. Teo, T. Chen, P. S. Lee, *ACS Nano* **2017**, *11*, 1712.
[65] W. Bai, R. Huang, Y. Cai, Y. Tang, X. Zhang, Y. Wang, *IEEE Electron Device Lett.* **2013**, *34*, 223.
[66] Y. Cai, J. Tan, L. YeFan, M. Lin, R. Huang, *Nanotechnology* **2016**, *27*, 275206.
[67] J. Ko, L. T. H. Nguyen, A. Surendran, B. Y. Tan, K. W. Ng, W. L. Leong, *ACS Appl. Mater. Interfaces* **2017**, *9*, 43004.
[68] B.-H. Lee, D.-I. Lee, H. Bae, H. Seong, S.-B. Jeon, M.-L. Seol, J.-W. Han, M. Meyyappan, S.-G. Im, Y.-K. Choi, *Sci. Rep.* **2016**, *6*, 38389.
[69] G.-T. Hwang, D. Im, S. E. Lee, J. Lee, M. Koo, S. Y. Park, S. Kim, K. Yang, S. J. Kim, K. Lee, K. J. Lee, *ACS Nano* **2013**, *7*, 4545.
[70] T. Sekitani, U. Zschieschang, H. Klauk, T. Someya, *Nat. Mater.* **2010**, *9*, 1015.
[71] C. K. Jeong, K.-I. Park, J. H. Son, G.-T. Hwang, S. H. Lee, D. Y. Park, H. E. Lee, H. K. Lee, M. Byun, K. J. Lee, *Energy Environ. Sci.* **2014**, *7*, 4035.
[72] D. H. Kim, H. G. Yoo, S. M. Hong, B. Jang, D. Y. Park, D. J. Joe, J.-H. Kim, K. J. Lee, *Adv. Mater.* **2016**, *28*, 8371.
[73] D. H. Kim, H. G. Yoo, D. J. Joe, K. J. Lee, presented at *Technical Digest – Int. Electron Devices Meeting, IEDM*, IEEE, Washington, DC, USA **2015**.
[74] S. H. Lee, J. Kim, J. H. Shin, H. E. Lee, I.-S. Kang, K. Gwak, D.-S. Kim, D. Kim, K. J. Lee, *Nano Energy* **2018**, *44*, 447.
[75] K. Takei, T. Takahashi, J. C. Ho, H. Ko, A. G. Gillies, P. W. Leu, R. S. Fearing, A. Javey, *Nat. Mater.* **2010**, *9*, 821.
[76] S. Choi, S. H. Tan, Z. Li, Y. Kim, C. Choi, P.-Y. Chen, H. Yeon, S. Yu, J. Kim, *Nat. Mater.* **2018**, *17*, 335.
[77] M. D. Ventra, Y. V. Pershin, *Nat. Phys.* **2013**, *9*, 200.
[78] B. Gao, Y. Bi, H.-Y. Chen, R. Liu, P. Huang, B. Chen, L. Liu, X. Liu, S. Yu, H. S. P. Wong, J. Kang, *ACS Nano* **2014**, *8*, 6998.
[79] P. A. Merolla, J. V. Arthur, R. Alvarez-Icaza, A. S. Cassidy, J. Sawada, F. Akopyan, B. L. Jackson, N. Imam, C. Guo, Y. Nakamura, B. Brezzo, I. Vo, S. K. Esser, R. Appuswamy, B. Taba, A. Amir, M. D. Flickner, W. P. Risk, R. Manohar, D. S. Modha, *Science* **2014**, *345*, 668.
[80] T. Ohno, T. Hasegawa, T. Tsuruoka, K. Terabe, J. K. Gimzewski, M. Aono, *Nat. Mater.* **2011**, *10*, 591.
[81] M. Ziegler, R. Soni, T. Patelczyk, M. Ignatov, T. Bartsch, P. Meuffels, H. Kohlstedt, *Adv. Funct. Mater.* **2012**, *22*, 2744.
[82] M. Abu Lebdeh, H. Abunahla, B. Mohammad, M. Al-Qutayri, *IEEE Trans. Circuits Syst.* **2017**, *64*, 2427.
[83] Y. Halawani, B. Mohammad, D. Homouz, M. Al-Qutayri, H. Saleh, *IEEE Trans. Very Large Scale Integr. Syst.* **2016**, *24*, 1003.
[84] B. Mohammad, D. Homouz, H. Elgabra, *IEEE Trans. Very Large Scale Integr. Syst.* **2013**, *21*, 2069.
[85] L. Nela, J. Tang, Q. Cao, G. Tulevski, S.-J. Han, *Nano Lett.* **2018**, *18*, 2054.
[86] S. Nie, Y. Yang, Y. He, Y. Shi, Q. Wan, *IEEE Electron Device Lett.* **2018**, *39*, 363.
[87] W. I. Park, B. K. You, B. H. Mun, H. K. Seo, J. Y. Lee, S. Hosaka, Y. Yin, C. A. Ross, K. J. Lee, Y. S. Jung, *ACS Nano* **2013**, *7*, 2651.
[88] G. Qin, Y. Zhang, K. Lan, L. Li, J. Ma, S. Yu, *ACS Appl. Mater. Interfaces* **2018**, *10*, 12798.
[89] R. Yao, Z. Zheng, Z. Fang, H. Zhang, X. Zhang, H. Ning, L. Wang, J. Peng, W. Xie, X. Lu, *J. Mater. Chem. C* **2018**, *6*, 2522.
[90] B. K. You, J. M. Kim, D. J. Joe, K. Yang, Y. Shin, Y. S. Jung, K. J. Lee, *ACS Nano* **2016**, *10*, 9478.
[91] S. G. Hu, Y. Liu, Z. Liu, T. P. Chen, J. J. Wang, Q. Yu, L. J. Deng, Y. Yin, S. Hosaka, *Nat. Commun.* **2015**, *6*, 7522.
[92] S. H. Jo, T. Chang, I. Ebong, B. B. Bhadviya, P. Mazumder, W. Lu, *Nano Lett.* **2010**, *10*, 1297.
[93] M.-K. Kim, J.-S. Lee, *ACS Nano* **2018**, *12*, 1680.
[94] Z.-H. Tan, R. Yang, K. Terabe, X.-B. Yin, X.-D. Zhang, X. Guo, *Adv. Mater.* **2016**, *28*, 377.

[95] S. Boyn, J. Grollier, G. Lecerf, B. Xu, N. Locatelli, S. Fusil, S. Girod, C. Carrétéro, K. Garcia, S. Xavier, J. Tomas, L. Bellaiche, M. Bibes, A. Barthélémy, S. Saïghi, V. Garcia, *Nat. Commun.* **2017**, *8*, 14736.
[96] C. Du, W. Ma, T. Chang, P. Sheridan, W. D. Lu, *Adv. Funct. Mater.* **2015**, *25*, 4290.
[97] Z. Q. Wang, H. Y. Xu, X. H. Li, H. Yu, Y. C. Liu, X. J. Zhu, *Adv. Funct. Mater.* **2012**, *22*, 2759.
[98] R. Yang, H. M. Huang, Q.-H. Hong, X. B. Yin, Z.-H. Tan, T. Shi, Y.-X. Zhou, X.-S. Miao, X. P. Wang, S. B. Mi, C. L. Jia, X. Guo, *Adv. Funct. Mater.* **2018**, *28*, 1704455.
[99] L. Q. Zhu, C. J. Wan, L. Q. Guo, Y. Shi, Q. Wan, *Nat. Commun.* **2014**, *5*, 3158.
[100] P. Krzysteczko, J. Munchenberger, M. Schafers, G. Reiss, A. Thomas, *Adv. Mater.* **2012**, *24*, 762.
[101] H. G. Yoo, S. Kim, K. J. Lee, *RSC Adv.* **2014**, *4*, 20017.
[102] Y.-W. Dai, L. Chen, W. Yang, Q.-Q. Sun, P. Zhou, P.-F. Wang, S.-J. Ding, D. W. Zhang, F. Xiao, *IEEE Electron Device Lett.* **2014**, *35*, 915.
[103] Y. Yang, G. Yuan, Z. Yan, Y. Wang, X. Lu, J.-M. Liu, *Adv. Mater.* **2017**, *29*, 1700425.
[104] S. Kim, J. H. Son, S. H. Lee, B. K. You, K.-I. Park, H. K. Lee, M. Byun, K. J. Lee, *Adv. Mater.* **2014**, *26*, 7480.
[105] J. Jang, F. Pan, K. Braam, V. Subramanian, *Adv. Mater.* **2012**, *24*, 3573.
[106] J. H. Park, S. Jeong, E. J. Lee, S. S. Lee, J. Y. Seok, M. Yang, Y. Choi, B. Kang, *Chem. Mater.* **2016**, *28*, 4151.
[107] H. Palneedi, J. H. Park, D. Maurya, M. Peddigari, G.-T. Hwang, V. Annapureddy, J. W. Kim, J.-J. Choi, B.-D. Hahn, S. Priya, K. J. Lee, J. Ryu, *Adv. Mater.* **2018**, *1705148*, 1.
[108] I. Choi, H. Y. Jeong, D. Y. Jung, M. Byun, C.-G. Choi, B. H. Hong, S.-Y. Choi, K. J. Lee, *ACS Nano* **2014**, *8*, 7671.
[109] K.-I. Park, J. H. Son, G. T. Hwang, C. K. Jeong, J. Ryu, M. Koo, I. Choi, S. H. Lee, M. Byun, Z. L. Wang, K. J. Lee, *Adv. Mater.* **2014**, *26*, 2514.
[110] G.-T. Hwang, V. Annapureddy, J. H. Han, D. J. Joe, C. Baek, D. Y. Park, D. H. Kim, J. H. Park, C. K. Jeong, K.-I. Park, J.-J. Choi, D. K. Kim, J. Ryu, K. J. Lee, *Adv. Energy Mater.* **2016**, *6*, 1600237.
[111] D. J. Joe, S. Kim, J. H. Park, D. Y. Park, H. E. Lee, T. H. Im, I. Choi, R. S. Ruoff, K. J. Lee, *Adv. Mater.* **2017**, *29*, 1606586.
[112] C. K. Jeong, S. B. Cho, J. H. Han, D. Y. Park, S. Yang, K.-I. Park, J. Ryu, H. Sohn, Y.-C. Chung, K. J. Lee, *Nano Res.* **2017**, *10*, 437.
[113] J. H. Park, G.-T. Hwang, S. Kim, J. Seo, H.-J. Park, K. Yu, T.-S. Kim, K. J. Lee, *Adv. Mater.* **2017**, *29*, 1603473.
[114] S. H. Sung, Y. S. Kim, D. J. Joe, B. H. Mun, B. K. You, D. H. Keum, S. K. Hahn, M. Berggren, D. Kim, K. J. Lee, *Nano Energy* **2018**, https://doi.org/10.1016/j.nanoen.2018.06.015.
[115] S.-T. Han, Y. Zhou, Q. D. Yang, L. Zhou, L.-B. Huang, Y. Yan, C.-S. Lee, V. A. L. Roy, *ACS Nano* **2014**, *8*, 1923.
[116] J. Liu, Z. Yin, X. Cao, F. Zhao, L. Wang, W. Huang, H. Zhang, *Adv. Mater.* **2013**, *25*, 233.
[117] S.-T. Han, Y. Zhou, C. Wang, L. He, W. Zhang, V. A. L. Roy, *Adv. Mater.* **2013**, *25*, 872.
[118] S. Kim, B. Choi, M. Lim, J. Yoon, J. Lee, H.-D. Kim, S.-J. Choi, *ACS Nano* **2017**, *11*, 2814.
[119] S. M. Kim, E. B. Song, S. Lee, J. Zhu, D. H. Seo, M. Mecklenburg, S. Seo, K. L. Wang, *ACS Nano* **2012**, *6*, 7879.
[120] W. J. Yu, S. H. Chae, S. Y. Lee, D. L. Duong, Y. H. Lee, *Adv. Mater.* **2011**, *23*, 1889.
[121] K. Nagashima, H. Koga, U. Celano, F. Zhuge, M. Kanai, S. Rahong, G. Meng, Y. He, J. De Boeck, M. Jurczak, W. Vandervorst, T. Kitaoka, M. Nogi, T. Yanagida, *Sci. Rep.* **2014**, *4*, 5532.
[122] M.-K. Kim, J.-S. Lee, *ACS Appl. Mater. Interfaces* **2018**, *10*, 10280.
[123] S. Yu, N. Xiao, M. Deng, Y. Xing, F. Liu, W. Chen, presented at *2017 Int. Conf. on Networking, Architecture, and Storage (NAS)*, IEEE, Shenzhen, China **2017**.
[124] P. Cappelletti, presented at *2015 IEEE Int. Electron Devices Meeting (IEDM)*, IEEE, Washington, DC, USA **2015**.
[125] W. Lu, C. M. Lieber, *Nat. Mater.* **2007**, *6*, 841.
[126] H. G. Yoo, M. Byun, C. K. Jeong, K. J. Lee, *Adv. Mater.* **2015**, *27*, 3982.
[127] S. H. Ko, H. Pan, C. P. Grigoropoulos, C. K. Luscombe, J. M. J. Fréchet, D. Poulikakos, *Nanotechnology* **2007**, *18*, 345202.
[128] S.-T. Han, Y. Zhou, V. A. L. Roy, *Adv. Mater.* **2013**, *25*, 5425.
[129] P. F. Moonen, I. Yakimets, J. Huskens, *Adv. Mater.* **2012**, *24*, 5526.
[130] T. Shimoda, Y. Matsuki, M. Furusawa, T. Aoki, I. Yudasaka, H. Tanaka, H. Iwasawa, D. Wang, M. Miyasaka, Y. Takeuchi, *Nature* **2006**, *440*, 783.
[131] R. A. Street, *Adv. Mater.* **2009**, *21*, 2007.
[132] B.-W. Chen, T.-C. Chang, K.-C. Chang, Y.-J. Hung, S.-P. Huang, H.-M. Chen, P.-Y. Liao, Y.-H. Lin, H.-C. Huang, H.-C. Chiang, C.-I. Yang, Y.-Z. Zheng, A.-K. Chu, H.-W. Li, C.-H. Tsai, H.-H. Lu, T. T- J. Wang, T.-C. Chang, *ACS Appl. Mater. Interfaces* **2017**, *9*, 11942.
[133] M. Kaltenbrunner, T. Sekitani, J. Reeder, T. Yokota, K. Kuribara, T. Tokuhara, M. Drack, R. Schwödiauer, I. Graz, S. Bauer-Gogonea, S. Bauer, T. Someya, *Nature* **2013**, *499*, 458.
[134] C. Wang, J.-C. Chien, K. Takei, T. Takahashi, J. Nah, A. M. Niknejad, A. Javey, *Nano Lett.* **2012**, *12*, 1527.
[135] D. Shahrjerdi, S. W. Bedell, *Nano Lett.* **2013**, *13*, 315.
[136] B. Crone, A. Dodabalapur, Y.-Y. Lin, R. W. Filas, Z. Bao, A. LaDuca, R. Sarpeshkar, H. E. Katz, W. Li, *Nature* **2000**, *403*, 521.
[137] D. K. Kim, Y. Lai, B. T. Diroll, C. B. Murray, C. R. Kagan, *Nat. Commun.* **2012**, *3*, 1216.
[138] D. Sun, M. Y. Timmermans, Y. Tian, A. G. Nasibulin, E. I. Kauppinen, S. Kishimoto, T. Mizutani, Y. Ohno, *Nat. Nanotechnol.* **2011**, *6*, 156.
[139] L. Sun, G. Qin, J.-H. Seo, G. K. Celler, W. Zhou, Z. Ma, *Small* **2010**, *6*, 2553.
[140] K.-L. Suk, H.-Y. Son, C.-K. Chung, J. D. Kim, J.-W. Lee, K.-W. Paik, *Microelectron. Reliab.* **2012**, *52*, 225.
[141] J. N. Burghartz, W. Appel, H. D. Rempp, M. Zimmermann, *IEEE Trans. Electron Devices* **2009**, *56*, 321.
[142] W. Christiaens, E. Bosman, J. Vanfleteren, *IEEE Trans. Compon. Packag. Technol.* **2010**, *33*, 754.
[143] A. R. Rathmell, B. J. Wiley, *Adv. Mater.* **2011**, *23*, 4798.
[144] M. W. Möller, D. A. Kunz, T. Lunkenbein, S. Sommer, A. Nennemann, J. Breu, *Adv. Mater.* **2012**, *24*, 2142.
[145] D. H. Kim, H. J. Shin, H. Lee, C. K. Jeong, H. Park, G.-T. Hwang, H.-Y. Lee, D. J. Joe, J. H. Han, S. H. Lee, J. Kim, B. Joung, K. J. Lee, *Adv. Funct. Mater.* **2017**, *27*, 1700341.
[146] H. S. Wang, C. K. Jeong, M.-H. Seo, D. J. Joe, J. H. Han, J.-B. Yoon, K. J. Lee, *Nano Energy* **2017**, *35*, 415.
[147] G.-T. Hwang, Y. Kim, J.-H. Lee, S. Oh, C. K. Jeong, D. Y. Park, J. Ryu, H. Kwon, S.-G. Lee, B. Joung, D. Kim, K. J. Lee, *Energy Environ. Sci.* **2015**, *8*, 2677.
[148] R. A. John, J. Ko, M. R. Kulkarni, N. Tiwari, N. A. Chien, N. G. Ing, W. L. Leong, N. Mathews, *Small* **2017**, *13*, 1701193.
[149] G. Indiveri, S.-C. Liu, *Proc. IEEE* **2015**, *103*, 1379.
[150] Z. Wang, S. Joshi, S. E. Savel'ev, H. Jiang, R. Midya, P. Lin, M. Hu, N. Ge, J. P. Strachan, Z. Li, Q. Wu, M. Barnell, G.-L. Li, H. L. Xin, R. S. Williams, Q. Xia, J. J. Yang, *Nat. Mater.* **2017**, *16*, 101.
[151] H. Tian, Q. Guo, Y. Xie, H. Zhao, C. Li, J. J. Cha, F. Xia, H. Wang, *Adv. Mater.* **2016**, *28*, 4991.
[152] M. Prezioso, F. Merrikh-Bayat, B. D. Hoskins, G. C. Adam, K. K. Likharev, D. B. Strukov, *Nature* **2015**, *521*, 61.
[153] S. Yu, B. Gao, Z. Fang, H. Yu, J. Kang, H.-S. P. Wong, *Adv. Mater.* **2013**, *25*, 1774.
[154] A. A. Bessonov, M. N. Kirikova, D. I. Petukhov, M. Allen, T. Ryhänen, M. J. A. Bailey, *Nat. Mater.* **2015**, *14*, 199.

[155] C. Wu, T. W. Kim, H. Y. Choi, D. B. Strukov, J. J. Yang, *Nat. Commun.* **2017**, *8*, 752.
[156] N. Liu, L. Q. Zhu, P. Feng, C. J. Wan, Y. H. Liu, Y. Shi, Q. Wan, *Sci. Rep.* **2016**, *5*, 18082.
[157] Y. S. Rim, H. Chen, B. Zhu, S.-H. Bae, S. Zhu, P. J. Li, I. C. Wang, Y. Yang, *Adv. Mater. Interfaces* **2017**, *4*, 1700020.
[158] D. Son, J. H. Koo, J.-K. Song, J. Kim, M. Lee, H. J. Shim, M. Park, M. Lee, J. H. Kim, D.-H. Kim, *ACS Nano* **2015**, *9*, 5585.
[159] N. Y.-M. Shen, Z. Liu, C. Lee, B. A. Minch, E. C.-C. Kan, *IEEE Trans. Electron Devices* **2003**, *50*, 2171.
[160] M. Koo, S. Y. Park, K. J. Lee, *Nanobiosensors Dis. Diagn.* **2012**, *1*, 5.
[161] S. I. Park, G. Shin, J. G. McCall, R. Al-Hasani, A. Norris, L. Xia, D. S. Brenner, K. N. Noh, S. Y. Bang, D. L. Bhatti, K.-I. Jang, S.-K. Kang, A. D. Mickle, G. Dussor, T. J. Price, R. W. Gereau, M. R. Bruchas, J. A. Rogers, *Proc. Natl. Acad. Sci. USA* **2016**, *113*, E8169.
[162] S. I. Park, D. S. Brenner, G. Shin, C. D. Morgan, B. A. Copits, H. U. Chung, M. Y. Pullen, K. N. Noh, S. Davidson, S. J. Oh, J. Yoon, K.-I. Jang, V. K. Samineni, M. Norman, J. G. Grajales-Reyes, S. K. Vogt, S. S. Sundaram, K. M. Wilson, J. S. Ha, R. Xu, T. Pan, T.-I. Kim, Y. Huang, M. C. Montana, J. P. Golden, M. R. Bruchas, R. W. Gereau, J. A. Rogers, *Nat. Biotechnol.* **2015**, *33*, 1280.
[163] H. Fang, K. J. Yu, C. Gloschat, Z. Yang, E. Song, C.-H. Chiang, J. Zhao, S. M. Won, S. Xu, M. Trumpis, Y. Zhong, S. W. Han, Y. Xue, D. Xu, S. W. Choi, G. Cauwenberghs, M. Kay, Y. Huang, J. Viventi, I. R. Efimov, J. A. Rogers, *Nat. Biomed. Eng.* **2017**, *1*, 38.
[164] J.-W. Jeong, J. G. McCall, G. Shin, Y. Zhang, R. Al-Hasani, M. Kim, S. Li, J. Y. Sim, K.-I. Jang, Y. Shi, D. Y. Hong, Y. Liu, G. P. Schmitz, L. Xia, Z. He, P. Gamble, W. Z. Ray, Y. Huang, M. R. Bruchas, J. A. Rogers, *Cell* **2015**, *162*, 662.
[165] C. Pang, G.-Y. Lee, T.-I. Kim, S. M. Kim, H. N. Kim, S.-H. Ahn, K.-Y. Suh, *Nat. Mater.* **2012**, *11*, 795.
[166] P. Horcajada, T. Chalati, C. Serre, B. Gillet, C. Sebrie, T. Baati, J. F. Eubank, D. Heurtaux, P. Clayette, C. Kreuz, J.-S. Chang, Y. K. Hwang, V. Marsaud, P.-N. Bories, L. Cynober, S. Gil, G. Férey, P. Couvreur, R. Gref, *Nat. Mater.* **2010**, *9*, 172.
[167] G.-T. Hwang, H. Park, J.-H. Lee, S. Oh, K.-I. Park, M. Byun, H. Park, G. Ahn, C. K. Jeong, K. No, H. Kwon, S.-G. Lee, B. Joung, K. J. Lee, *Adv. Mater.* **2014**, *26*, 4880.
[168] G.-T. Hwang, M. Byun, C. K. Jeong, K. J. Lee, *Adv. Healthcare Mater.* **2015**, *4*, 646.
[169] S.-W. Hwang, H. Tao, D.-H. Kim, H. Cheng, J.-K. Song, E. Rill, M. A. Brenckle, B. Panilaitis, S. M. Won, Y.-S. Kim, Y. M. Song, K. J. Yu, A. Ameen, R. Li, Y. Su, M. Yang, D. L. Kaplan, M. R. Zakin, M. J. Slepian, Y. Huang, F. G. Omenetto, J. A. Rogers, *Science* **2012**, *337*, 1640.
[170] H. E. Lee, J. Choi, S. H. Lee, M. Jeong, J. H. Shin, D. J. Joe, D. Kim, C. W. Kim, J. H. Park, J. H. Lee, D. Kim, C.-S. Shin, K. J. Lee, *Adv. Mater.* **2018**, https://doi.org/10.1002/adma.201800649.
[171] C. Dagdeviren, Y. Shi, P. Joe, R. Ghaffari, G. Balooch, K. Usgaonkar, O. Gur, P. L. Tran, J. R. Crosby, M. Meyer, Y. Su, R. C. Webb, A. S. Tedesco, M. J. Slepian, Y. Huang, J. A. Rogers, *Nat. Mater.* **2015**, *14*, 728.
[172] K.-I. Jang, H. U. Chung, S. Xu, C. H. Lee, H. Luan, J. Jeong, H. Cheng, G.-T. Kim, S. Y. Han, J. W. Lee, J. Kim, M. Cho, F. Miao, Y. Yang, H. N. Jung, M. Flavin, H. Liu, G. W. Kong, K. J. Yu, S. I. Rhee, J. Chung, B. Kim, J. W. Kwak, M. H. Yun, J. Y. Kim, Y. M. Song, U. Paik, Y. Zhang, Y. Huang, J. A. Rogers, *Nat. Commun.* **2015**, *6*, 6566.
[173] L. Gao, Y. Zhang, V. Malyarchuk, L. Jia, K.-I. Jang, R. C. Webb, H. Fu, Y. Shi, G. Zhou, L. Shi, D. Shah, X. Huang, B. Xu, C. Yu, Y. Huang, J. A. Rogers, *Nat. Commun.* **2014**, *5*, 4938.
[174] R. Yu, C. Pan, J. Chen, G. Zhu, Z. L. Wang, *Adv. Funct. Mater.* **2013**, *23*, 5868.
[175] H. S. Lee, J. Chung, G.-T. Hwang, C. K. Jeong, Y. Jung, J.-H. Kwak, H. Kang, M. Byun, W. D. Kim, S. Hur, S.-H. Oh, K. J. Lee, *Adv. Funct. Mater.* **2014**, *24*, 6914.
[176] R. Saran, R. J. Curry, *Nat. Photonics* **2016**, *10*, 81.
[177] H. Deng, X. Yang, D. Dong, B. Li, D. Yang, S. Yuan, K. Qiao, Y.-B. Cheng, J. Tang, H. Song, *Nano Lett.* **2015**, *15*, 7963.
[178] T. Wang, Y. Guo, P. Wan, H. Zhang, X. Chen, X. Sun, *Small* **2016**, *12*, 3748.
[179] S. H. Lee, C. K. Jeong, G.-T. Hwang, K. J. Lee, *Nano Energy* **2015**, *14*, 111.
[180] S. Jung, J. Lee, T. Hyeon, M. Lee, D.-H. Kim, *Adv. Mater.* **2014**, *26*, 6329.
[181] W. Xu, S.-Y. Min, H. Hwang, T.-W. Lee, *Sci. Adv.* **2016**, *2*, e1501326.
[182] S. Ju, A. Facchetti, Y. Xuan, J. Liu, F. Ishikawa, P. Ye, C. Zhou, T. J. Marks, D. B. Janes, *Nat. Nanotechnol.* **2007**, *2*, 378.
[183] L. S. Liyanage, H. Lee, N. Patil, S. Park, S. Mitra, Z. Bao, H. P. Wong, *ACS Nano* **2012**, *6*, 451.
[184] M. J. Cima, *Nat. Biotechnol.* **2014**, *32*, 642.